The application of 3D image registration techniques in diagnosis and therapy

Jing Yi Wang

A report submitted to the University College London
for the award of the qulified to the Mphil degree

2001

Department of Medical Physics and Bioengineering

University College

University of London

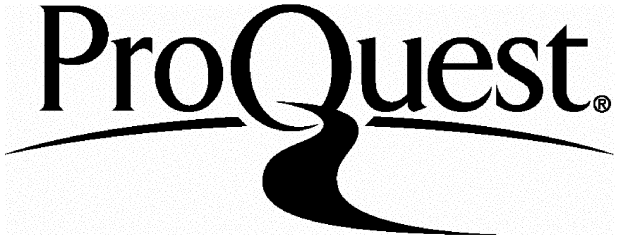

Abstract

In recent years, rapid developments in medical 3D scanner technology have led to a major increase in the amount of information available to the physician. Image data are acquired using techniques like CT, MR, SPECT and PET. In this thesis, I will give a general review of the base technique of registration and its clinical applications; report on using an image fusion technique to integrate these 3D multimodality images to develop a clinical therapy planning tool.

The first aim of my project was to investigate the use of different kinds of registration methods on a group of children. Different kinds of registration methods are reviewed. The clinical on applications are discussed and some of our new work is reported.

The second aim of our project was to produce registered and subtracted ictal and interictal SPECT images obtained from the children. In order to highlight the lesions, the transformed, normalised interictal images were subtracted from the normalised ictal image to create an image where the value for each pixel represents the intensity difference between the two data sets. The standard deviation (SD) of the distribution of the subtraction pixel intensities was calculated, and the subtraction image thresholded to display only pixels with values greater than 2 SDs above zero. Ictal SPECT provides unique information on the dynamic changes in regional cerebral blood flow (rCBF) that occur during seizure and, thus, could be useful in clarifying the poorly understood interplay of the interictal states in human focal epilepsy. The results were compared with the visual diagnosis and surgical outcome and enhanced the ability to localize the seizure foci.

The future work will be based on improving the accuracy of the method of normalisation. The threshold range selection will be further investigated for different injection times. The size of the subtraction image highlights which correspond to the lesions will need further investigation

Acknowledgements

I would like to thank my principal supervisor Dr. A.D.Linney for his great support and encouragement throughout the duration of this thesis. I am also grateful my second supervisor Dr. Cliff Ruff for his helpful suggestions. There are many friends and colleagues who provided invaluable encouragement both on a practical and emotional level. In particular, I would like to thank Dr. Jing Deng for his friendship when I first arrived at the Medical Graphics and Imaging Group and for patiently teaching me the basic knowledge of how to use the computer and software. I am also grateful to the people in the Medical Graphics and Imaging Group for their support. I would also like to thank Dr. Isky Gordon for providing me with the SPECT data and related clinical information.

Finally but not at least I would like to thank my husband Jie Sun for his financial support and my daughter Yi Yang for being very good company during these years.

Table of Contents

List of Tables

List of Figures

List of Symbols

x	Rectangular coordinates of a location within an imaged scene
Vm	The set of points making up the volume of material imaged by modality M
m(x),n(x)	The underlying value exhibited by a material at location x
m(x),n(x)	The measured value of a physical property at location x
R	The set of regions of material making up a scene being imaged
k,K	A set of points making up a region in the image all exhibiting the same value of a property
M,N	Sets of values of properties exhibited materials in a scene
p(m)	Probability of a value *m* occurring within an imaged scene
M,N	Sets of measurement values
p(m)	Probability of a measurement value *m* occurring within an image
T	A transformation mapping between two 3D images of a scene
$б'_{n(m)}$	Normalised standard deviation of corresponding image values N with respect to the image values M
H(M)	Entropy of a set of symbols $m \in M$
H(M,N)	Joint entropy between sets of measured values M and N
I(M,N)	Mutual information between sets of measured values M and N
Y(M,N)	Normalised Mutual information between sets of measured values M and N

List of Abbreviations

3D	Three Dimensional
2D	Two Dimensional
CBF	Cerebral Blood Flow
CT	(X-ray) Computer Tomography
EEG	Electroencephalography
FDG	Fluorodeoxyglucose Radiopharmaceutical used in PET imaging
FRE	Fiducial Registration Error
FWHM	Full Width at Half Maximum
HMPAO	Hexamethylpropylene amine oxime: Radiopharmaceutical used in SPECT imaging
MR	Magnetic Resonance
PET	Positron Emission Tomography
SAVD	Sum of Absolute Value Different
SD	Standard Deviation
SPECT	Single Photon Emission Computer Tomography
SVD	Singular Value Decomposition
TLP	Temporal Lobe Epilepsy
TRE	Target Registration Error
VOI	Volume Of Interest

Chapter 1
Introduction

The work described in this thesis is concerned with the application of registration of 3D medical images. In particular it deals with the task of using this procedure for help diagnose epilepsy in children. The aim is to investigate the reliability of using registered SPECT ictal and interictal subtraction images to display the lesion locations. It concentrates on the tasks by reviewing the best way for registering, normalising and thresholding the SPECT images. Other clinical applications are also discussed in this thesis.

1.1 The Clinical Requirement

There is an ever increasing range of clinical imaging modalities available, each measuring distinctly different properties or characteristics of material within the patient. This thesis is mainly concerned with the alignment of 3D volumetric images of the head that are acquired for a number of clinical applications. The main 3D imaging modalities dealt with in this thesis are:

- Single Photon Emission Computed Tomography (SPECT) Imaging
- Positron Emission Computed Tomography (PET)
- Nuclear Magnetic Resonance (MR) Imaging
- Computed Tomography (CT) X-ray Imaging

Each of these modalities can be tuned to distinguish significantly different properties within the body by varying acquisition parameters and imaging protocol for example:

- Chemical Tracer and Isotope Distribution
- MR Enhancement Chemical (for example Gadolinium) Distribution
- MR Plus Special Sequences
- X-ray Energy Absorption

Different settings of these parameters may provide significantly different contrast between them and so produce a distinctly different 'modality' . This is particularly true for MR images where modification of echo times and methods of data acquisition can produce

images delineating white matter, grey matter, cerebrospinal fluid, blood flow or even brain function. An important limitation is that even these images cannot in general be acquired simultaneously, and therefore because of unknown patient movements between scans, cannot be assumed to be spatially aligned.

Different physical measurements may provide significantly different contrast between tissues and so produce a distinctly different 'modality'. The location and repositioning of these modalities are of critical importance to medical imaging. In the past, it has been common for physicians to interpret data from different modalities, recorded at different times, using a poorly described yet generally understood visual alignment system. This in effect involves applying some spatial transformation between structures within an image in order to match the data. Decisions as to the progress of disease and other important medical issues are often based on this process. Such an approach is questionable, even given the high degree of spatial sense possessed by many physicians. The need exists for more objective methods of aligning image information [3].

1.2 An overview of the thesis

The thesis can be divided into two main parts. The first part in chapters 2 and 3 deal with the general review of the work which has been done by the others. The thesis begins with a review of the registration techniques presented in chapter 2. The basic classification techniques of the registration and the strategy of how to select the method are summarised in the first section. The following section pays attention to a review of conventional approaches to image registration based on the extraction and alignment of corresponding features.

The clinical application areas, which include using registration techniques first, and then fusion or image subtraction, to produce the required diagnostic or treatment planning information, are described in chapter 3. In this chapter, I have generally reviewed the clinical applications based on some kind of reported disease or treatment and present some work which I have carried out.

The second main part consists of chapters 4, 5 and 6. An imaging modality which is particularly considered is SPECT. SPECT is a valuable clinical tool in the management of epilepsy patients who are under evaluation for surgical treatment. An interictal SPECT study is important for accurate interpretation of ictal studies. SPECT perfusion scans are traditionally analysed by visually comparing each interictal and ictal image. There are potential difficulties that arise when ictal, and interictal perfusion scans are compared in the conventional manner. We used a method which uses image registration and applies a normalisation to account for variability in brain uptake and total injected activity based on a single slices and the subtraction of the ictal and interictal SPECT data. The significant

changes during the seizure are calculated by displaying only pixels with values greater than 2SDs above zero in the subtractual image. The methodology and evaluation is described in chapter 4. In this chapter we also describe the method which has been used for selecting the best registration method to register the images including cases where brain volume changes due to growth have occurred between image acquisitions.

In chapter 5, we will assess this method for clinical practice. We describe the fusion of the subtraction image with the MR images. The result is compared with the visual diagnosis and surgical outcome. This study shows that the technique may enhance the ability to localise epileptic seizure foci. The study is based on eleven children who were patients suffering from epilepsy at Great Ormond Street Hospital.

In chapter 6, the future ideas for research will be based on improving the method which we have used. The normalisation and threshold range selection will be further examined and we will develop new methods which are more accurate for use on children at different times with respect to tracer injection. The lesion size and location assessment will need further investigation.

Chapter 2
General review of registration technique

2.1 Technique background

2.1.1 Dimensionality

Any registration method will produce a set of equations that transform the co-ordinates of each point in one image into the co-ordinates of the (physically) corresponding point in the other image.

Spatial registration can be performed in any dimension. In 2-D methods, projection images or tomographic slices of different recordings are aligned, assuming that the images are made exactly in the same plane relative to the patient. 3-D methods consider a tomographic image not as a set of individual slices but as a volumetric data set that can be registered with another (2-D or 3-D) image. Methods may include time as an extra dimension. A one-dimensional (1-D) method may perform a temporal match on a time series of spatially consistent images. Matching of a time series of 3-D images becomes a 4-D method [7]. Matching time series of 2-D images then becomes a 3-D method.

When 2-D methods are used for registration of data obtained from 3D subjects, it is assumed that the images to be matched are made exactly in the same plane and, for projections, also projected from the same point or direction, all relative to the patient. To meet this assumption, special patient positioning requirements are needed, which complicates the clinical imaging protocol. This is especially true for tomographic modalities, where small variations in patient positioning may result in large changes in a tomographic slice.

2.1.2 Domain of the transformation

The transformation that maps the co-ordinate system of one image onto the other can be either global or local. A matching transformation is called global when a change in any one of the matching parameters influences the transformation of the image as a whole. Local matching transformations may vary in granularity from voxel-sized to organ-sized.

2.1.3 Use of image properties

Registration algorithms may either use intrinsic, e.g., patient related image properties or

extrinsic image properties by including artificial objects that are attached to the patient. Intrinsic properties are, for example, pixel intensities, anatomical landmark points, geometrical features, or surfaces of skin, cortex, or ventricles, and materials administered to the patient to enhance contrast for diagnostic purposes. Extrinsic properties are, for example, head frames or skin markers.

With registration methods using intrinsic properties, it is assumed that similar structures can be extracted from both images to be matched. This is not a trivial task, especially for images carrying complementary information (such as CT and MR) or in pathological cases. Manual extraction of intrinsic properties, for example in landmark matching, is labour-intensive, while (semi-automatic) extraction of, for example, surfaces tends to be complicated. Since with intrinsic methods no special measures are necessary in the imaging protocol, the methods are patient-friendly.

With registration methods based on extrinsic properties, it is assumed that for each modality a marker can be constructed that is visible in the images, without affecting the diagnosis. Usually, construction of markers complying with this requirement is not a problem, although materials for such a marker have to be chosen with care. Extrinsic properties are generally extracted from the images with more ease than are intrinsic properties, because the design of extrinsic markers can be optimised for automatic detection. An additional advantage is that, in general, matching results can easily be checked visually by comparing the positions of the markers in the images. An obvious disadvantage of extrinsic methods is that they require special procedures and protocols.

In both intrinsic and extrinsic matching methods it is assumed that the transformation that aligns the image properties also adequately registers the entire region of interest. It follows that methods producing relatively complex transformations, such as local and/or curved transformations, need a sufficiently large, properly distributed set of image properties. This requirement implies that methods using markers outside the body, which usually is the case in extrinsic methods, are less suited for matching of, for example, images with geometric deformations, such as the abdomen.

2.1.4 Categories of the transformations

The matching transformation can be rigid, affine, projective, or curved. These categories, indicating the degree of elasticity of the transformation, have been selected such that they show a clear distinction in geometrical properties. A transformation is called rigid if the distance between any two points in the first image is preserved when these two points are mapped onto the second image. Rigid transformations can be decomposed into translation, rotation, and (mirror) reflection. In3-D, the point(x, y, z)=[X] is transformed into the point (x'

y' z')=[X'] using the formula

$$[X']=[X][T]. \tag{2.1}$$

[T]=[Tr][Rx][Ry][Rz]=

$$\begin{pmatrix}1&0&0&tx\\0&1&0&ty\\0&0&1&tz\\0&0&0&1\end{pmatrix}\begin{pmatrix}1&0&0&0\\0&\cos\sigma&\sin\sigma&0\\0&-\sin\sigma&\cos\sigma&0\\0&0&0&1\end{pmatrix}\begin{pmatrix}\cos\theta&0&-\sin\theta&0\\0&1&0&0\\\sin\theta&0&\cos\theta&0\\0&0&0&1\end{pmatrix}\begin{pmatrix}\cos\beta&-\sin\beta&0&0\\\sin\beta&\cos\beta&0&0\\0&0&1&0\\0&0&0&1\end{pmatrix} \tag{2.2}$$

where[Tr] denotes the translation matrix. [Rx],[Ry],[Rz] denotes the rotation matrix and σ, θ, β denotes the rotation angle of x-axis,y-axis and z-axis, and the tx, ty, tz are translation vector.

A transformation is called affine when any straight line in the first image is mapped onto a straight line in the second image, while parallelism is preserved. Affine transformations can be decomposed into a linear (matrix) transformation and a translation.

$$\begin{pmatrix}x'\\y'\\z'\\1\end{pmatrix}=\begin{bmatrix}A_{11}&A_{12}&A_{13}&tx\\A_{21}&A_{22}&A_{23}&ty\\A_{31}&A_{32}&A_{33}&tz\\0&0&0&1\end{bmatrix}\begin{pmatrix}x\\y\\z\\1\end{pmatrix} \tag{2.3}$$

where

$$\begin{bmatrix}A_{11}&A_{12}&A_{13}&tx\\A_{21}&A_{22}&A_{23}&ty\\A_{31}&A_{32}&A_{33}&tz\\0&0&0&1\end{bmatrix}$$

denotes any real-valued matrix.

A projective (or perspective) transformation maps any straight line in the first image onto a straight line in the second image; parallelism between straight lines is in general not preserved. Projective transformations can be represented by matrix transformation in a higher dimensional space (3D or 4D).

$$\begin{pmatrix}x'\\y'\\z'\\1\end{pmatrix}=\begin{bmatrix}A_{11}&A_{12}&A_{13}&A_{14}\\A_{21}&A_{22}&A_{23}&A_{24}\\A_{31}&A_{32}&A_{33}&A_{34}\\A_{41}&A_{42}&A_{43}&A_{44}\end{bmatrix}\begin{pmatrix}x\\y\\z\\1\end{pmatrix} \tag{2.4}$$

Curved transformations may map a straight line onto a curve.

$$(x',y')=F(x,y) \tag{2.5}$$

where F denotes any function mapping the co-ordinates in the first image onto co-

ordinates in the second image. A well-known class of curved transformation functions are the transformations of polynomial type. A second order nonlinear model as below :

$$X' = a_{00} + a_{10}x + a_{01}y + a_{20}x^2 + a_{11}xy + a_{02}y^2 + \ldots.$$
$$Y' = b_{00} + b_{10}x + b_{01}y + b_{20}x^2 + b_{11}xy + b_{02}y^2 + \ldots.$$
$$Z' = c_{00} + c_{10}x + c_{01}y + c_{20}x^2 + c_{11}xy + c_{02}y^2 + \ldots. \quad (2.6)$$

A consequence of the above categorisation into rigid, affine, projective, and curved mappings is that rigid transformations are a subset of affine transformations, which in turn are a subset of projective transformations, which in turn are a subset of curved transformations. Rigid transformations thus are curved transformation with zero elasticity.

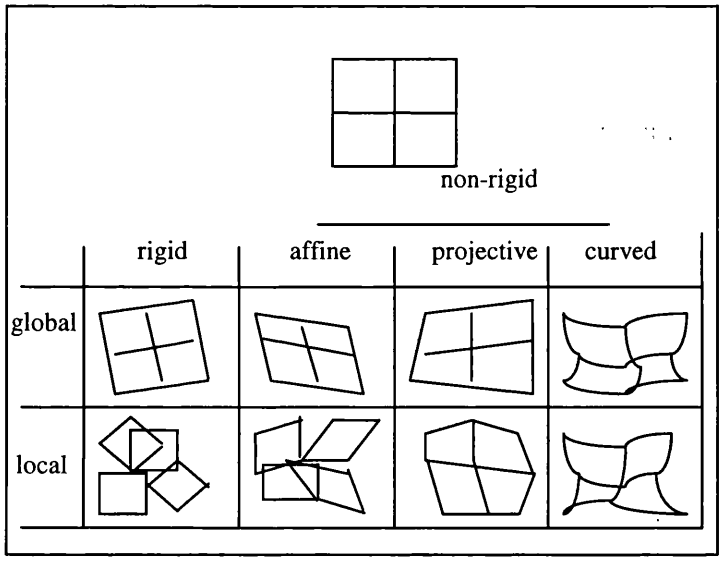

Fig. 2.1 *Example of 2D image transformations supported by the combined domain and elasticity categories. All local transformation may induce gaps or overlaps. Local affine, projective, and curved transformations can be restricted so that gaps or overlaps do not occur.*

It is assumed that the type of transformation used in the matching is adequate to describe the actual displacement and deformation of the body part under study. In order to choose the right combination of image domain and transformation elasticity criteria, some information is needed. For example, machine dependent image distortion, machine calibration errors, elasticity of the body parts that are scanned, and movement of organs under study. Only then, the type of transformation can be chosen to suit properly the specific application.

Global rigid matching suffices for relatively stable objects, such as one patient's head in different modalities, even in MR where small patient- as well as machine-induced distortions are inherent. All other transformation types may introduce distortions that were not present in the images beforehand, especially when image matching properties are scant or unreliable. This is why for relatively stable objects, such as a human brain, rigid transformations are generally preferred. At first, local rigid transformations seem practically useless, because the transformed image contains gaps that are not present in the original images to be matched. A

hypothetical situation where local rigid transformations may be useful is a multimodal or time study of one patient skeleton in which each local region corresponds to a bone.

Global affine matching is, for example, suitable for stable objects when image scaling or gantry tilt information is missing or unreliable. Projective transformations are almost exclusively used to register projection (X-ray) images to 3-D tomographic images, employing a 3-D to 2-D variant of the projective formula.

Transformations that are curved and/or local with reasonably high granularity may be used when one of the images has to be deformed to fit the other image, as in matching patient data with atlas data or in matching objects that change shape in between scans. e.g., in abdominal studies, brain growth studies.

2.1.5 Tightness of property coupling

The transformation that relates two images can be directing or approximating. Directing transformations precisely map image properties in the first image onto properties in the second image. Approximating transformations distribute the matching error over all properties, for example by a least-squares fit.

In directing methods, it is assumed that the image properties used for matching are located precisely. Any error made in locating an image property will reduce the accuracy of the resulting transformation proportionally over (part of) the image. In medical images, precise localisation of image properties seems unrealistic, owing to coarse sampling in one or more of the dimensions of the image, the limited resolution of the imaging device, the complementary nature of the information in images of different modalities, and noise. In approximating methods, it is assumed that the errors in the location parameters of the image properties have zero mean.

2.1.6 Resampling and interpolation

Different imaging systems may derive an estimate of the value of a property from different volumes of material. In order to carry out a registration more inexpensively, a resampling step prior to alignment ensures that the images have comparable spatial resolution and sampling rate in each axis (Fig 2.2). This process is carried out by reducing the spatial resolution of images where one is appreciably higher resolution than the other.

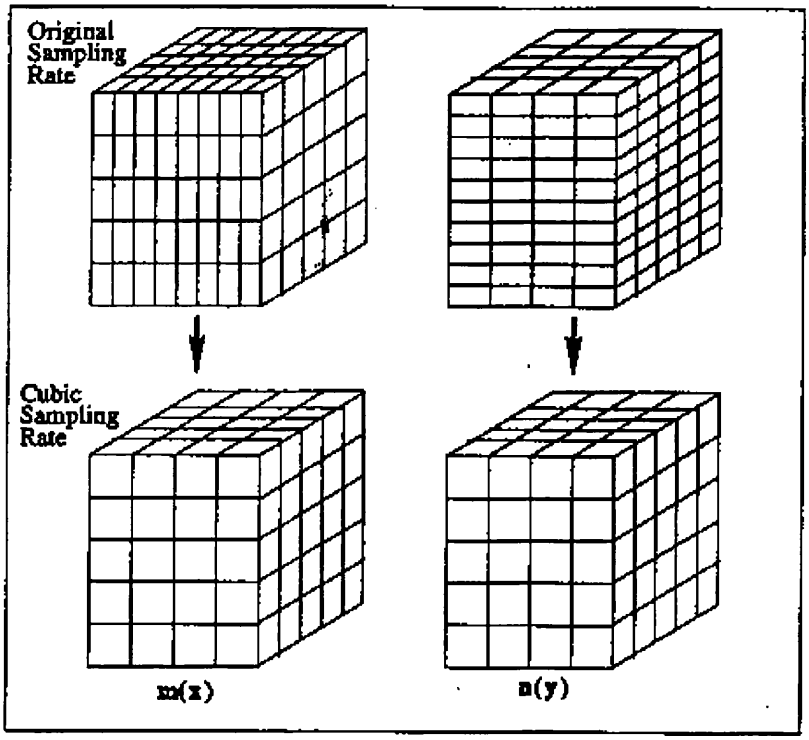

Fig.2.2 *An illustration cubic resampling of 3D images prior to alignment*

The process of the transformation using the interpolation technique. The accuracy of an interpolation value is governed by the extent of the kernel support used to derive the estimate. The most accurate interpolation is achieved with a sinc kernel of large extent. When kernel size is reduced the interpolation accuracy falls. Increase kernel size, on the other hand will need a large mount of computation. As a result, some people choose to limit the interpolation overhead by using a simple piecewise linear kernel. For the 3D, tri-linear interpolation is often used.

2.1.7 Parameter determination

A registration algorithm may be direct or search-oriented. A direct method straightforwardly computes the transformation parameters. A search-oriented method starts from one or more initial guesses, and tries to find the optimal transformation, guided by a goodness-of-match measure.

Direct methods are usually based on lists of corresponding points. In both direct and search-based matching methods that use point-to-point matching, accuracy generally increases with the number of used points.

In direct methods, it is assumed that the problem of finding the best match is simple enough to allow for straightforward calculation. Often this is not the case, and simplifications

of the problem are made to bring the complexity down to a level that does allow straightforward calculation.

In the search-oriented method, a measure may be better at extreme misregistration .

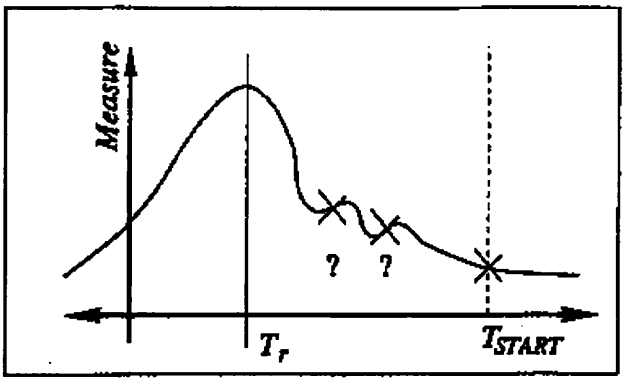

Fig. 2.3 *An illustration of a parameter space where the 'capture range' for even a simple uphill search is not easy to define because of local optima where the gradient may be reversed.*

This is due to the volume of overlap decrease as misregistration continues to increase. The quantity of image structure over which the registration measure is evaluated therefore falls. Thus, in searching for true registration, one needs to find a local optimum of any measure. In general a valid starting estimate is provided by the imaging protocol itself, in that a specific region of interest, such as a tumour is imaged by both modalities. It is assume that the centre of the two imaged volumes are roughly aligned and this single starting estimate is within the capture range of the measure, and the final optimum lies 'up hill' from that estimate. The problem is then one of searching up hill from this starting estimate avoiding local optima on the way, as illustrated in Fig 2.3.

Multi-resolution techniques offer advantages during iterative registration. One of them is increasing speed through computational efficiency. This is due to lower the resolution of the images being fully represented by a smaller number of measurement values. Another is that the robustness to local optima can be achieved by the blurring of smaller objects and fine structure when the resolution is lower. These regions in the image correspond to merging of smaller peaks with larger ones in the joint histogram. The result is the single sharp peak instead of the multi-smaller peaks when the resolution continues to decrease.

In order to improve the starting estimate a simple iterative optimization scheme is used. Given a starting estimate T0 described by six rigid transformation parameters, a similarity measure is evaluated for a set of transformations T(T0). These are the current starting estimates and the starting

estimates with increments and the decrements of each of the 3 translations (T) and 3 rotations (R) until a better estimate is found. Because the accuracy of the estimate is limited by the spatial resolution of the images the step size is then be reduced and the search resumed in order to further refine the estimate. The initial step size should be chosen properly and the smallest step size is chosen experimentally as being appreciably smaller than the errors in the final registration estimate due to other factors.

2.1.8 Interaction

A reasonably rigorous classification of degree of interaction can be divided into three categories: interactive, semi-automatic, and automatic. Interactive methods need human intervention for the determination of the transformation. In semi-automatic methods, a computer programme determines the transformation, while user interaction is required for the selection of image properties to be used in the registration, and/or for starting, guidance, or stopping of the matching procedure. Automatic methods need no human interaction as indicated before, many registration methods of widely varying degree of interaction are classified as semi-automatic. It should be noted that the amount of interaction needed may highly affect the practical usefulness of a method. However, user interaction should not always be judged unfavorably; a small amount of interaction may simplify or speed up the matching task considerably, or increase its reliability. In interactive or semi-automatic procedures, it is assumed that the available operator is trained for the task. They may, for example, be assumed to have medical or mathematical skills or sufficient ability to reason about 3-D geometry. The matching results of methods employing human interaction may suffer from user subjectivity.

2.2 Literature review based on registration technique

In order to describe the spatial relationship between two 3D image volumes we need a transformation T which relates points y={x, y, z} in one image space say Vn to points x={x, y, z} in the other, say Vm, so that,

$$X = T(y). \qquad (2.7)$$

2.2.1 Corresponding point alignment

The most direct approach to registration is to first identify corresponding pairs of landmarks in the two images, and then to bring these points into alignment. If we can identify some corresponding pairs of points within the two images, then we can consider each of these point pairs to be a solution to alignment. If we have enough of these point pairs we can use them to find the value of T describing the alignment of the two images. Effectively, knowing the location of a subset of all pairs of points in the images allows us to find the transformation for the whole image. Mathematically the process of aligning the two sets of K selected points $X = \{x_i\}$ and $Y = \{y_i\}$, where $i = 1,\ldots, K$, can be expressed as simply minimising the mean square distance,

$$Dp(T) = \sum_{i=1}^{k} \| x_i - T(y_i) \|^2 , \qquad \text{between each pair.}$$

How can we find the transformation for the whole image based on these points? One of the most flexible and clinically applicable approaches to image registration has been that based on manual, interactive, point landmark identification [12]. The availability of more powerful computing resources allows the use of interactive display tools to considerably simplify the process of point location. An obvious approach to semi-automated or automated registration is to develop a system capable of calculating the transformation parameter after interactive point selection or automated selection [30]. One of the more popular approaches is a well-known technique which uses singular value decomposition (SVD) to find a least-squares fit of homologous points [16].

Landmark making and identification

The landmarks identification can be obtained by using extrinsic or intrinsic image properties.

Different kinds of stereotactic frames have been used as extrinsic landmarks. For example, four small markers attached to the intracranial holes made for the stereotactic frame, to (globally, rigidly) calculate the 3-D stereotactic coordinates. Fiducial markers fastened to an individually cast face mask have also been used. Another method uses triangular markers on the skin which can be located semi-automatically in tomographic images with subslice accuracy, which makes this approach especially suitable for matching standard clinical CT and MR datasets containing thick slices and/or large interslice gaps [4]. A variety of extrinsic markers have been developed for different modalities. For example, plastic moulds are made for each external auditory meatus and the glabella. A pocket is then made in each mould in

which either a ^{57}Co disk(for SPECT) or an identical disk containing $CuSO_4$ solution (for MR) can be placed [9]. Following the performance of one or more transmission scans, radioactive fiducial markers were taped onto ink-marker skin sites on the patient that were expected to be within the field of view of the scanner. These fiducial markers contained 0.5-3 mCi of FDG adsorbed onto ~2-5 mm diameter polystyrene beads. Vitamin E capsules were taped over the same marked skin sites used for the MR scanner. Small cylindrical lead markers, roughly 2 mm in diameter x 1.0cm in length, were placed over the same marked skin sites for the CT scans [8].

In the literature, a great variety matching lists of corresponding intrinsic point pairs is described. A number of direct methods for multimodalities [30] or affine brain image to atlas matching [4] have been described which use a small number of landmarks and assume a certain amount of uniformity in brain structure. The intrinsic landmarks are usually chosen carefully to be special anatomic features which can be seen on both modalities.

For the extrinsic landmark method, on some occasions, some markers were not included in the field of view of both scans. On the other hand, the use of internal landmarks is subject to errors due to the variable physiologic states in the case of functional images. Since most point-to-point type registration procedures may use (extrinsic) marker points or (intrinsic) landmark points, some authors use both. Richard [8] used a rigid rotate-translate scale model and realignment algorithm based on operator-identification of external markers and unique anatomic points defined on both transmission PET images and the anatomic images. Maguire, et al. [12] used a fully interactive method based on extrinsic markers and/or intrinsic landmarks to reduce their 3-D registration problem to 2-D.

2.2.2 Corresponding surface alignment

An alternative, and more feasible task than the automated identification of anatomical landmarks, is the extraction of points on a corresponding boundary in both images. If it is possible to extract the same surface from the two modalities, then it is possible to derive an estimate of the alignment between the pair of images, as illustrated in Fig 2.4

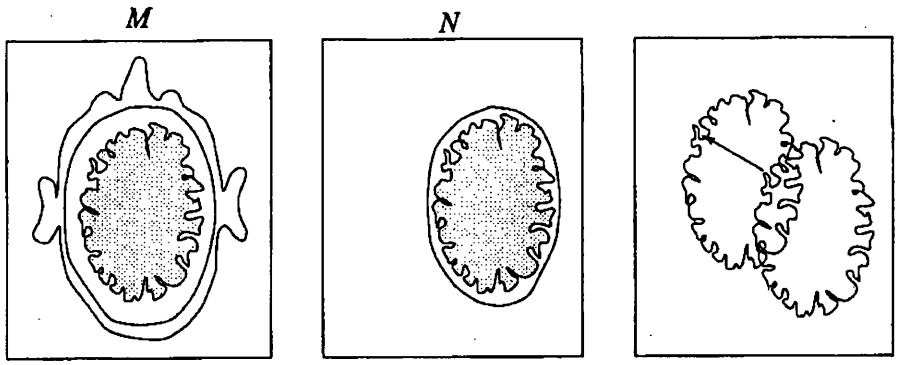

Fig 2.4 : *Extraction of the corresponding surfaces between which a measure of mis-alignment may be derived.*

Surface matching can be thought of as the problem of aligning two sets of points where the one-to-one correspondence of pairing is unknown. Given a pair of point sets,

$$X = \{x_i\} \quad \text{where } i = 1,2,....K$$
$$Y = \{y_j\} \quad \text{where } j = 1,2,....L \qquad (2.9)$$

describing surfaces X and Y respectively. Even if the surfaces exactly correspond, at registration the points on the surfaces are not necessarily aligned and, even the number of points on the surfaces need not be the same. Because we do not have any point correspondence information, we need, for a given point xi, a function for the transformation T which returns a corresponding co-ordinate on the other surface described by the set Y, say $P(T(Y),xi)$. This may simply be the nearest point in the second set or a more complex description (for example a point on the triangulation of surface points Y). Given this function, we can then develop a measure similar to that for point matching, based on the overall distance between the surface,

$$Ds(T) = \sqrt{\sum_{i=1}^{k} || x_i - P(T(Y), x_i)||^2} \quad . \qquad (2.10)$$

The alignment by finding the value of T which minimises $Ds(T)$ requires an iterative search. The difference between point based alignment and surface based alignment is that point based alignment is truly a measure of the distance from correct alignment of the two corresponding point sets. Surface based alignment on the other hand, is not a direct 'distance to registration' but, simply a measure of the alignment of the two surfaces.

Surface identification and handing

How do we identify corresponding surfaces? Some researchers do this by the choice of

the skin surface which is relatively easy to extract. The two problems posed by this are the accuracy of rigid alignment estimates due to skin surface deformation, and the robustness of the matching due to symmetries and lack of the fine structure in the skin surface. Some workers employ manually initiated extraction of the brain boundary from MR and SPECT and PET where the skin surface extraction is more difficult. For MR-CT registration, skull boundaries are extracted from MR for matching with those from CT by histogram thresholding at 15% and 65% at the maximum MR value by one group [38]. Hill [39] was the first to use neighbouring surface to derive a registration estimate. This work illustrated registration using alignment of the inner skull surface extracted from CT and the outer brain surface extracted from MR.

Handing outliners is another important aspect of matching surfaces. If the outliers in one object are different from another, these could shift the correct optimum leading to error in alignment. One approach to this problem is to specifically exclude regions were differences occur, but again this generally requires some form of manual intervention. Some groups employed a simple form of thresholding, to exclude the influence of outliers, distances to nearest points were simply thresholded to a particular value chosen experimentally.

Surface matching approaches

Chen, Pelizzari, and co-workers, developed a popular 3-D parametric correspondence method to register tomographic brain images. A surface module (head) extracted from one image is related to a set of points (hat) extracted from contours in another image by a rigid and optionally affine transformation [16]. The "hat" is fitted on the "head" by a search strategy that uses a least squares fit. In order to make the task easier, the approach employs a number of simplifications. The contribution to the residual for each "hat" point is evaluated by finding the intersection with the "head" surface of a ray from the transformed "hat" point to the centroid of the "head" model. This approach assumes, given the centroids are initially aligned, that the two surfaces are predominantly spherical, so that the ray directions defined from the centroid are close to the true nearest point direction. Sufficient surface should be scanned to prevent the problem from being ill-posed. An accuracy of the order of one to two pixels of the image with the lowest resolution has been achieved in phantom studies for CT, MR, and PET.

This method has been used successfully at several clinical sites. The surface matching technique is evaluated in the spatial correlation of SPECT and MR cardiac images [7]. The method is based on matching corresponding anatomical surfaces extracted from transmission SPECT and MR studies. Patients with brain tumours were studied on one or more occasions using MR and high resolution FDG-PET to analyse the brain tumour [18] [40]. PET-CT alignment using this method has been reported to help diagnose lung cancer patients [41].

The evaluation of the goodness-of-match function used by a parametric correspondence method can be optimised for speed by applying a distance transform to the static image using the "chamfering" method [38]. Rather than represent the two surfaces to be matched simply by two lists of points, one of the objects delineated can be stored as a binary image where voxels or pixel values are either object or background. From this binary image, a distance image, can be formed using a 'distance transform' where each voxel or pixel outside the object is given a value representing its distance to the nearest point on the object. To evaluate the overall distance between two objects for a given transformation, the set of points describing the object in one image is simply transformed to locations in the distance image of the other object. The method has been used for SPECT- CT image registration [38].

2.2.3 Combining different types of geometrical feature

One of the major criticisms of feature based approaches is that they are using only a small part of information available in the images to determine image alignment. In many cases a surface may not constrain the registration adequately or there may be inadequate numbers of corresponding points in the images to provide an accurate estimate. Recently there has been considerable interest in using different types of geometrical features in determining 3D alignment.

Pietrzyk, et al. [10] manually determined a 3-D transformation relating two tomographic brain images. Aided by both separate and fused displays of multiple slices from the images to be matched. Seitz et al. [11] used interactive methods for local curved matching of atlas contours with patient images. Some methods solve a 3-D registration problem in two steps, either of which may be interactive. Kapouleas et al.[13] first semi-automatically aligned the mid-sagittal planes using indicated end points of the midline in all relevant axial MR and PET brain slices, then the remaining 2-D translation and rotation were determined manually by aligning the overlaid outline of each sagittal MR slice on the corresponding resliced PET image. Yaorong [14] described a registration method similar to that of Kapouleas et al. except that, in the second step, equivalent points are identified by the user and the collection of paired points from multiple parasagittal slices is registered using a simple least-squares minimisation algorithm.

A number of approaches have been proposed to include structural information in the matching process, e.g., curves, planes [15] [17]. All methods reviewed based on structures use intrinsic image properties and generate global approximating transformations: most methods are semi-automatic.

2.2.4 Moments/principal axes matching

A frequently used approach in image matching is based on moment matching techniques. Volumes [20] and surfaces or scattered points [4] can all be used with moment matching. From the moments of inertia, the principal axes of the object can be derived. Translation is calculated from the position of the centroid of an object or a set of landmarks (equal to the first order moments), and rotation is calculated by aligning the object's or landmark population's principal axes of inertia (equal of the second order moments), which renders this technique direct. Moments matching techniques produce approximating transformations because they are based on statistical principles. Furthermore, as many points are needed, in practice only intrinsic properties are used. Generally, the approach is semi-automatic as some user interaction is needed to extract the image properties.

Moment matching techniques will result in inaccurate rotational parameters when, because of symmetry, there are no unique principle axes. This absence seems more probable with landmarks than with surfaces or volumes in medical applications. Differences in the scanned volume and large slice spacing may affect all parameters if a significant part of the volume of the object is missing in one or both of the scans. The result may therefore be unreliable in specific pathological cases, for example when matching functional images showing peripheral metabolic deficiencies with images depicting anatomy.

2.2.5 Image similarity as a measure of alignment

A similarity can be derived from the global relationship between voxel values in the two modalities. The basic idea is that two values m and n are related or similar simply if there are many other examples of those values occurring together in the overlapping imaged volume. Effectively it can be said that in aligning the images the transformation is changed in order to increase the clustering of the joint probability distribution so that there are few low probability pairs and more higher probability pairs. In terms of the delineated regions, a transformation is sought which maximises clustering for the volume of the majority of the interesting region. We can express an overall image similarity S for a transformation T between the two images, as the sum of individual measurement similarities $S(.)$, at Q different points

$$S(T) = \sum_{i=1}^{Q} S(\mathrm{m}(\mathrm{x_i}), \mathrm{n}(T(\mathrm{x_i}))) , \quad (2.11)$$

where m(xi) and n(T(xi)) are corresponding values. We would like S to be a monotonic function of misalignment, which behaves like a mean distance between features. For this to be the case, the number of pairs $\sum^{Q}{}_{i=1} S(.))$ should fall smoothly with misalignment. We must therefore assume that there are uniform regions of corresponding values in the two images at

alignment. In many cases this is a valid assumption for many 3D medical modalities. The key question in this approach is then how do we say whether values in the modalities are similar, i.e. what do we use for our function *S(.)*?

Multi-modality imaging is the process of using measurements of different physical properties to delineate different regions of material in the body. We can refer to a single modality as providing a view of the underlying scene. It is the unknown relationship between these views which forms the basic problem of multi-modality alignment.

In this case, unlike conventional computer vision problems, the view of the scene differs not because of camera angle or the removal or introduction of objects, but simply because of the difference in the property being imaged. A related field is that of multi-spectral remote sensing, where it is conventional for images at different wavelengths to be acquired simultaneously and therefore in correspondence. In medical imaging such an arrangement is unlikely to be feasible either technically or financially in a clinical setting.

We can image the scene with a device which will make measurements of a property at points $x \in Vm$. The device will record the actual underlying values $m(x)$ as an image of measurement m(x). Here a value falls within the set M of possible values and a measurement within the set M of possible measurements. Examples of properties imaged for medical use are:

- X-ray linear attenuation coefficient μ
- Radioisotope density resulting from tracer uptake in tissues
- Proton spin density and relaxation times

A scene may be divided into sets of points (which are termed regions) which exhibit a particular value,

$$\psi(m) = \{ x \mid x \in Vm, m(x) = m\}. \quad (2.12)$$

The complete image consists of the set of regions delineated by each of the occurring value $m \in M$

$$M(M) = \{k \mid k = \psi(m), m \in M\}. \quad (2.13)$$

The regions M are determined by the properties $m \in M$, of each of the anatomical or physiological classifications $r \in R$ summarised by the mapping,

$$\phi : R \rightarrow M. \quad (2.14)$$

If there exists a simple one-to-one mapping from classification of material to properties of those materials, then we have an ideal modality which can delineate all the regions of interest within the patient. In practice this is often not the case, and the imaged property does not distinguish all the regions needed for a clinically sufficient description. Here there will be one or more pairs of regions which exhibit the same values of the property so that the mapping is not one-to-one.

As a result a second modality is often used to provide an image $n(x)$ of a measurement of a second property $n \in N$, for which the mapping $\phi: R \rightarrow N$ will be different. This new image will then delineate a second set of regions $N(N)$ as illustrated in Fig 2.5

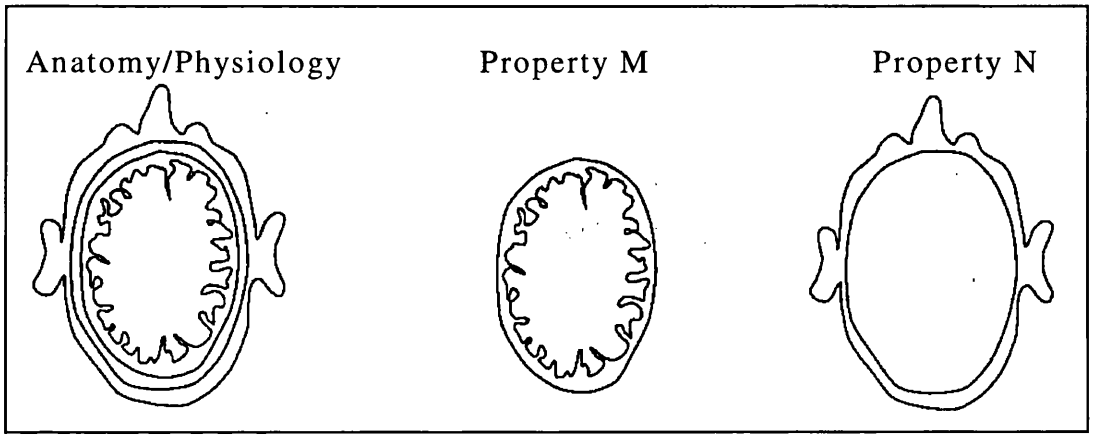

Fig 2.5 *Alternative 'view' of structure within a volume provided by measurement of different properties.*

A representation which captures the relationships between volumes of all regions delineated by a pair of images is the joint histogram of values. For each pair of values of two properties, the number of points at which those values occur together in the imaged volume of overlap is recorded in a 2 dimensional array, resulting in a direct estimate of the matrix. By normalising each volume by the total imaged volume of overlap, $Vo(T) = v\ (Vm \cap T(Vn))$ we can form a joint probability distribution

$$P(M,N) = \frac{1}{Vo(T)}\ U(T). \qquad (2.15)$$

Here, individual elements,

$$P(M, N) = \begin{bmatrix} p\{m_1,n_1\}p\{m_1,n_2\}.....p\{m_1,n_j\} \\ p\{m_2,n_1\}p\{m_2,n_2\}.....p\{m_2,n_j\} \\ .. \\ p\{m_i,n_i\}p\{m_i,n_2\}.....p\{m_i,n_j\} \end{bmatrix} \qquad (2.20)$$

represent the probability of occurrence of individual pairs of values in the images region.

From this we can extract the marginal probability distributions of the sets of values in each view of the scene alone,

$$p\{m\} = \sum_{n \in N} p\{m, n\}, \qquad (2.21)$$

and

$$p\{n\} = \sum_{m \in M} p\{m, n\}. \qquad (2.22)$$

Sum of absolute value difference (SAVD)

The simplest and most direct measure of similarity of two image values is given by their absolute difference. An overall measure of alignment may then be determined by the average absolute difference over each of the Q measurement points,

$$SAVD(T) = \frac{1}{Q} \sum_{i=1}^{k} || m(x_i) - n(T(x_i)) || \qquad (2.23)$$

In applying this measure we are assuming that the image values are effectively calibrated to the same scale so that corresponding objects exhibit the same measurement value. If this is the case then SAVD will tend to zero at alignment, if this is not the case then the behaviour is less predictable, depending on the measurement values delineating the largest regions. It is interesting to consider the amount of influence that a boundary between two regions has on the overall measure for two transformations say *T1* and *T2* [43]. Equation 2.23 shows that it will obviously depend on the difference of values across the boundary $n(T1(x_i))$-$n(T2(x_i))$. The overall influence is dependent on the length and orientation of the boundary. The influence though does not depend on the size of the objects at either side of the boundary. High contrast boundaries between small objects may therefore have a greater influence on the measure than low contrast boundaries between large objects.

SAVD is ideal in cases where two images are identical expect for noise. Example applications include the alignment of images acquired to investigate the progression or regression of disease, or changes in the chemical state in the brain. Application of this approach to aligning other modalities where image values are not directly related is limited. Even the simplest application of matching one MR image to another of the same sequence is complicated by the varied scaling between two seemingly identical acquisitions.

This method has been used for SPECT and PET studies of phantoms and patients [43]. The technique is relatively unaffected by localised differences in activity distribution and the range of noise in clinical studies.

Correlation

In the simplest case of within modality registration, for example aligning two MR images of the same sequence, registration results in a strong linear relationship between corresponding values in two images. Misalignment then breaks down this relationship as different values over-lie each other. In this case an obvious measure of similarity *S(.)* would be one which determines a linear fit to the distribution of corresponding values. In deriving a match from the fit of the data to a line of any gradient, we can avoid the problems of intensity scaling experienced with the SAVD measure.

This approach is employed in the most commonly used measure of image alignment, correlation, and is expressed simply as the sum of the product of all the pairs of values in the images,

$$\gamma\,(T) = \sum_{i=1}^{Q} m(x_i).n(T(x_i)) \qquad (2.24)$$

There are two basic limitations of this function when used as a measure of image alignment. Firstly, it is not independent of the number of points over which it is evaluated. In comparing two transformations, there may be significantly different regions of overlap between the imaged volumes, and so appreciably different numbers of points Q available for evaluation of γ. In such a case the correlation would tend to be greater for the transformation resulting in the greater volume of overlap. This can be avoided simply by dividing γ by the number of points,

$$\gamma'\,(T) = \frac{r(T)}{Q} \qquad (2.25)$$

to provide an estimate of the normalised cross correlation. A further problem is that

Equation 2.25 is also not independent of the overall level of the signal in the region of overlap and so the measure would tend to favour alignments which include larger image values. As a result, a better measure of alignment of finite images is the Correlation Coefficient where we consider the mean values of the two images over the set of Q points. Mathematically the correlation coefficient is a measure of the residual errors from the fitting of a line to the data by minimisation of least squares. In the field of signal processing the correlation of a signal with a known signal is template matching. Matching filtering or convolution is simply the correlation of a signal with a known signal reflected along each of its axes. Correlation would be expected to be useful only for image types where the relationship between values in the two images is predominantly linear at registration.

Correlation based methods map regions of pixels on a best-fit basis, and therefore are approximating, and always search-based and intrinsic [21][22]. Grey value correlation of original pixel intensities is generally not useful for multimodality matching, as pixel intensities in different modalities are usually not functions of correlating parameters.

Variance of intensity ratio

This is a simple statistical measure proposed by Woods [69] for aligning one PET image to another of the same patient. Empirically, when the pair of images are correctly aligned then for each of corresponding values in the images, the ratio,

$$r_i(T) = \frac{m(x_i)}{n(T(x_i))}. \qquad (2.26)$$

of their values is evaluated. The standard deviation of this ratio σr is evaluated over all i voxel pairs. This is then normalised by dividing by the mean value r' of each of the voxel pairs,

$$R = \frac{\sigma_r}{r'} \qquad (2.27)$$

giving a final measure of alignment which is minimised at registration. This is closely related to the correlation coefficient and assumes that there is a constant scaling factor relating the values in one image to the other at registration.

Corresponding intensity variance

Woods proposed the minimisation of corresponding variance for multi-modality registration of MR and PET imagery of the brain. To align the images, the algorithm seeks to minimise the standard deviation of the PET pixel values that correspond to each MR pixel value. We can work out for all voxels in image m(x), say with value m, the mean value of the

corresponding voxels in the second image n(T(x)), say Nm. Similarly we can find the standard deviation of those values бn(m). For a particular value m then we can work out the normalised standard deviation,

$$б_{n(m)} = б_n(m)/ Nm. \qquad (2.28)$$

The standard deviation of the distribution of intensities n for each intensity m should be minimised at registration. Given a probability of occurrence for each value m, say p(m), a weighted sum of the normalised standard deviation of the values N corresponding to each MR value $m \in M$,

$$б(N)=\sum_{m \in M} p(m)\, б'_n(m). \qquad (2.29)$$

provides a measure of alignment. The weighting ensures that the measure is influenced most strongly by PET intensity variation for the most common MR values.

The basic assumption this approach makes is that, at registration, uniform regions in one image map to uniform regions in the other. As the images move away from alignment, measuring the spread of corresponding values by their variance gives a direct measure of alignment. In practice this though may be approximately true for images where there are only small differences.

If for two images at registration, one value maps to two significantly different values in the other modality, then a measure of the clustering around the mean value will provide a poor indication of alignment. The degree to which there is a direct one to one mapping between values in the two images will determine the applicability of this measure. In order to ensure a close to one-to-one mapping of values in his application, Woods employed a simple MR segmentation to exclude non-brain regions, particularly scalp, from the measure.

What is also important is the direction of the mapping, i.e. choosing to minimise corresponding variance in the first or second modality can make a significant difference. One modality, say MR, may delineate significantly more regions than say PET and so every value in the MR may map to only one value in the PET (expect perhaps a small region of physiological abnormality), while the reverse is not true.

Imran [44] has used Woods method to assess the accuracy and reliability for standardization of brain SPECT images of patients with Alzheimer's disease. There was significantly decreased regional cerebral blood flow in the frontal, parietal, and temporal regions in the patient group, more marked in those patients having severe dementia. Imran [45] also used this method for standardised cerebral blood flow (CBF) images for a

comparision of patients and control subjects and for covariance analyses.

Moments of the joint probability distribution

This was first proposed by Hill et al. [46] from visual examination of the effects of misregistration on the feature space. Empirically, as the images approach registration, the peaks in the joint probability distribution increase in the height and the regions which contain lower counts decrease in height. The registration process is re-arranging the voxels so that they occur with their most probable corresponding value in the other image, given the constraints of the image structure and the transformation.

One approach to quantifying this shift from more low values in p{m,n} to more high values in p{m,n} is to measure skewness in the distribution of probabilities in p{m,n}. Common measures of skewness in the distribution are provided by the higher order moments of the distribution. Given p{m,n} we can calculate the number of occurrences of a particular probability p, say $\eta(p)$. The moment of order i of this distribution can then be evaluated:

$$g_i(M,N) = \int_0^1 \eta(p).p^i \, dp \qquad (2.30)$$

This can be normalised by dividing by the zero moment or mass.

$$g_0(M,N) = \int_0^1 \eta(p) \, dp \qquad (2.31)$$

Hill proposed the use of the third order moment as a measure of MR and CT alignment which is simply:

$$g_3(M,N) = \frac{g_3(M,N)}{g_0(M,N)} \qquad (2.32)$$

This has been compared experimentally to the joint entropy measure and found to provide similar response to alignment of MR and PET images of the brain.

Joint entropy and image alignment

If we examine the probabilities of values occurring in an image, it is common for there to be a range of probabilities, since some values are rare and some are common. In predicting what value a voxel has we can form an estimate of the uncertainty of our guess at the value given the observed distribution of probabilities. If we learn the value of a measurement that we were very uncertain about (i.e. it would be difficult to guess) then we gain a large amount of information. If we are given a set of values we can then look at the average amount of information provided by the set of values. The most commonly used measure of information which satisfies these requirements though is the Shannon-Weiener entropy measure. Here the average information supplied by a set of i symbols whose probabilities are given by

{p1,p2,....pi}, can be expressed as,

$$H(p1,p2,.....,pi) = -\sum_{i=1}^{i} p_s \log p_s . \qquad (2.33)$$

When two views of a scene are combined by a transformation mapping from points in one view to the other, the joint probability distribution tells us how often pairs of values occur together. The information content of this combined scene can be evaluated in a similar way to that of a scalar scene by forming an estimate of the joint entropy from the joint probability distribution,

$$H(M,N) = -\sum_{n \in N} \sum_{m \in M} p\{m,n\} \log (p\{m,n\}). \quad (2.34)$$

The use of joint entropy as a measure of multi-modality image alignment has been proposed independently in two original papers [62] [63]. In aligning different modalities we wish to use any shared features in the two images to define the registration. If structures are shared between the two images and the images are mis-aligned, then in the combined image these structures will be duplicated. For example, when a transaxial slice through the head is mis-aligned, there may be four eyes and four ears. As the images are brought into alignment the duplication of features is reduced and the combined image is simplified.

We can think of the 'combined' image, where pairs of values occur together, as a single valued image where each different value corresponds to a particular pair of values in the two source images. We may then express the joint probability distribution as a 1D vector, where each probability is simply derived from the size of each intersecting region. We increase the area of the larger aligned part and decrease the area of smaller mis-aligned parts. In using entropy as a measure of alignment we are making one important assumption: that the large regions in the two images are to be aligned and their region of overlap should increase as the images approach registration. If there are large regions in both images, but at alignment their overlap is not maximised, then joint entropy will not be a minimum at registration.

Mutual information

If we take a closer look at the use of joint entropy as a measure of alignment, we can see in practice that there is a problem. In bringing two images into alignment we are interested in essentially comparing two alignments to decide which is better. In deriving a measure of alignment from images with limited field of view (often in the clinical case, very limited) then any measure of structure or 'information content' of the combined image will be a function of the structure in the two images in their region of overlap. By minimising joint entropy we are

simply trying to find the combined image which delineates least structure, not necessarily the most corresponding structure. A second and related problem can be seen by considering the larger scale behaviour of the measure as mis-alignment increases. As we continue to misregister we would hope the measure will continue to degrade, tending toward a maximum of joint entropy. For general medical images this is obviously not the case, and in fact as misalignment increase, tissue in one modality overlies air in the other. What we need to do is to relate changes in the value of the joint entropy back to the marginal entropies of the two images alone. The approach described by Collignon [47], appears the most promising. The measure of mutual information used in communication theory to describe the information carried by a communication channel, by relating the information content of the transmitted and received signals. By treating the images as sources of information, information theory provides the basic tools for describing and developing generic measures of alignment. Simply, this expresses the joint entropy with respect to the marginal entropies.

$$I(M,N) = H(M) + H(N) - H(M,N). \qquad (2.35)$$

From this representation, remembering that the probabilities are derived from volumes of overlapping regions, *I(M, N)* relates the size of the overlap of a pair of regions (p{m,n}), to their total size (p{m} and p{n}).

This method was tested by Meyer [48] in a demonstration of accuracy and clinical versatility for automatic multimodality image fusion. They used a thorax phantom with PET/CT scans, PET/MR brain scans with significant missing data and abdominal SPECT/CT scans. Mean error vector lengths for rotate-translate registrations were measured to be subvoxel in phantoms. More importantly the rotate-translate algorithm performs well even with missing data. The demonstrated clinical fusion was qualitatively excellent at all levels. Kim [49] has used the mutual information method to provide accurate motion correction for multislice functional magnetic resonance imaging in clinical applications.

Normalising mutual information

The fundamental problem in using mutual information for our application is that it was developed in communication theory as a direct measure of the quantity of information passed between transmitter and receiver. For any given channel this will be dependent on the information transmitted. In our application we wish to compare an information measure derived for two transformation estimates. These estimates will correspond to different overlaps of the two image volumes, and therefore the amount of transmitted (and received) information may very between the two transformations simply because of the change in

overlap.

In order to account for changes in the proportion of mutual information we want to look at the amount of mutual information, with respect to the information provided by the individual images. A direct approach to normalisation proposed in this work is to evaluate the ratio of the joint and marginal entropies:

$$Y(M,N) = \frac{H(M)+H(N)}{H(M,N)} . \qquad (2.36)$$

Chapter 3

Clinical applications - A general review and clinical approach

In the literature, most authors apply image registration techniques to the brain. In the case of the brain, where the organ boundaries are typically constrained by the skull, methods based on organ outlines or areas will also work well. In other organs where organ geometry can be distorted by gravity and posture, the problem is more difficult and may indeed by intractable. In the case of anatomic atlases which attempt to locate subregions within an organ, normal anatomy, or at least the absence of these effects, is a requirement. The clinical application areas include using registration techniques first and then fusion or image subtraction to produce the required diagnostic or treatment planning information. In this chapter, I will generally review the clinical applications based on different kinds of disease or treatments and decribe some experiments which I have carried out.

3.1 Registration for cancer research

Registration and subtraction of MR images has been used to detect increases and decreases in tumour size following treatment (Fig 3.1). Some patients undergo both MR/CT imaging and PET of the brain because these modalities reveal complementary information. For example, MR/CT imaging may be used to produce an optimal depiction of brain anatomy, but it provides little insight into brain function. PET images may be acquired to visualise aspects of local brain function but do not adequately delineate brain anatomy. The feasibility of using PET to characterise tumours has been demonstrated most extensively for tumours of the brain. Several more advantages of PET in brain tumour diagnosis have been demonstrated. PET is used in determining the degree of malignancy of a tumour and in determining the prognosis of brain tumour patients. PET is useful in determining the appropriate biopsy site in patients with multiple lesions, large homogeneous lesions, and large heterogeneous lesions. PET is accurate in differentiating recurrent tumour from necrosis in patients who have undergone radiation therapy and chemotherapy. PET has also been successful in determining the prognosis of patients with brain tumours and PET has also been shown to predict survival in patients with gliomas more accurately than either CT or MR [35].

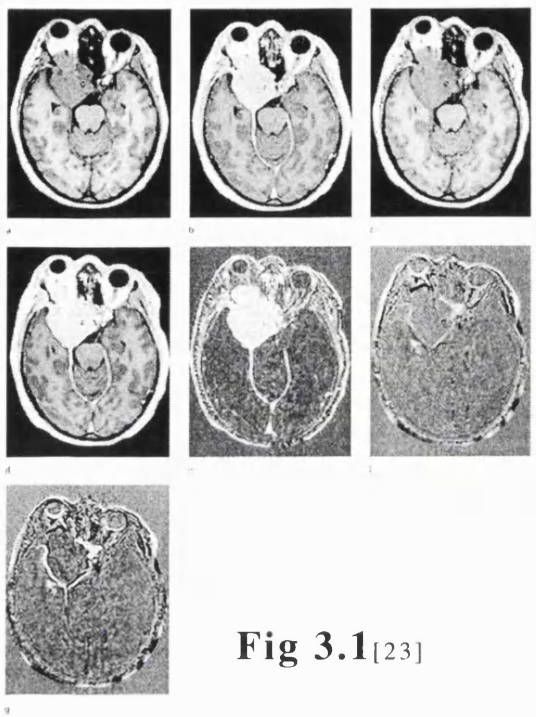

Fig 3.1[23]

Registration may allow earlier recognition of tumour growth and response to therapy than conventional techniques. A cohort of inoperable and partially resected meningiomas to assess their rate of growth has been studied[23].

Fig 3.1 is a meningioma patient: T1 weighted images from volume acquisitions before (a) and after (b) contrast enhancement; registered images at the same level before (c) and after (d) contrast enhancement 13 months later. Subtraction of (c) from (d) show the pattern of enhancement on the second examination in (e). Subtraction of (a) from (c) in image (f) shows that the tumour has grown over the 13 months between the scans. The same changes are seen with the addition of the effect of contrast enhancement in (g), which is (d)-(b).[23]

To assess the significance of combining such data, Sarsh [18] used surface-matching techniques to 21 adult patients with brain tumours for whom the correlation of anatomic and functional information was needed for clinical evaluation. Because the low grade tumours or small high grade tumours would be difficult to differentiate from normal grey matter and some patient's prior radiation therapy might cause difficulty in interpreting the significance of absolute levels of FDG uptake due to partial voluming of necrosis and active tumour. The registration of MR and PET images was found to be particularly helpful in these circumstances.

There is a increase in the FDG uptake region in the PET which corresponds to the enhanced area in the MR image. The registered MR and PET images in Fig 3.2 demonstrate that the alignment was particularly valuable in identifying a region of necrosis or oedema as defined by PET. For the MR, the area of contrast enhancement on the MR was seen to provide a larger area than PET. The outside area can be interpreted as oedema or necrosis.

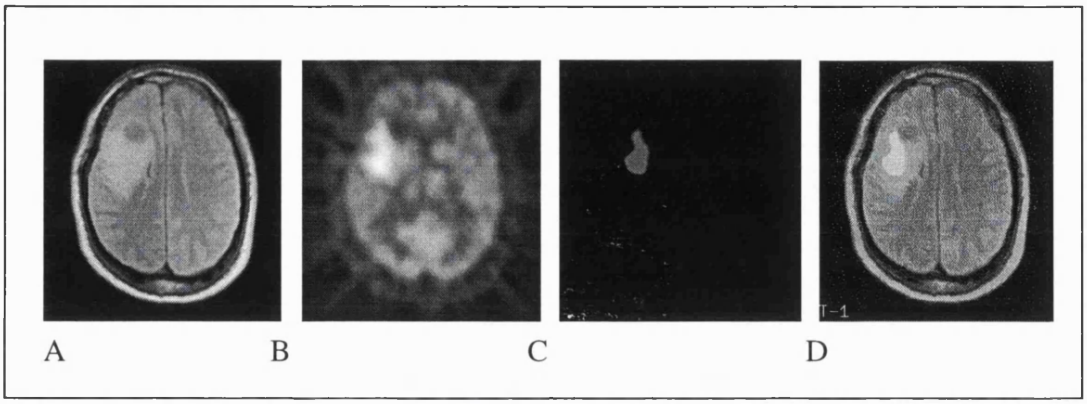

Fig 3.2 *(A) is the MR image, (B) is the corresponding PET image, (C) is the tumour highlight obtained from (B) using segmentation method ,(D) is the(C) fused with (A).*

The ability to make direct correlation between MR anatomy and uptake of PET using 18F-FDG images allows an improved appreciation of the morphological and functional characteristics of tumour tissue and another kinds of lesion (necrosis or oedema). A side-by-side comparison is important in gaining an overall assessment of the location and extent of regions of abnormal image intensity associated with brain tumours, both at a particular time point during therapy and at sequential examinations. Such evaluations are particularly relevant when the normal anatomy is distorted by mass effects or when the absolute levels of FDG uptake are equal to or lower than that of normal gray matter. Thus, the registration of PET and MR images may help resolve clinical issues concerning the significance of focal MR lesions and subsequent PET results by allowing enhanced understanding of the anatomic/spatial associations between the two studies.

In the evaluation of the cancer patient, radiolabeled antibody imaging can provide unique information which is unavailable through any other imaging modality currently in use. Gerald and Maguire[12] have fused SPECT, CT, and MR for evaluation of hemangiomas using monoclonal antibodies (MoAbs) with SPECT and CT for localisation of colo-rectal carcinomas and staging of non-small-cell lung carcinoma. Elissa has fused radiolabeled monoclonal antibody SPECT with CT in patients with colo-rectal or lung cancer [27]. Loat s[28] reported that he used the external body fiducial landmarks to study the metastatic malignancies in the gastrointestinal tract. Andrew [29] used a similar method to study patients with metastatic thyroid cancer. The presence of hepatic metastases from thyroid cancer has been confirmed by this technique.

3.2 Registering real patient with images for surgery planning

A frameless stereotactic arm can be used in conjunction with computerised tomography (CT) or magnetic resonance (MR) imaging to provide image-based intraoperative navigation. Surgical techniques using stereotactic frames permit neurosurgeons to perform biopsies and to resect deep-seated and previously inaccessible lesions. These frame-based techniques, however, have several limitations. The stereotactic frames themselves are bulky and may interfere with the surgical exposure. Patients complain about the weight of the frame and the pain associated with its application.

All frame-based and frameless systems rely on transformation of the digital data of imaging studies to the stereotactic space of the operative field. In conventional frame-based systems, the frame provides fiducial points that are visualised on the imaging study. These points define the stereotactic space by virtue of the rigid attachment of the frame to the patient's head. In frameless systems, the patient's scalp itself has been used as a fiducial marker. When the position of the markers is measured with a digitising device, it can be correlated with the position of the markers on the imaging study. From this correlation, the imaging data can be transformed to the stereotactic space of the operative field. The position of the tip of the digitising device is said to be registered with the imaging data so that any point on the patient's head can be mapped to its corresponding point in the imaging study and vice versa [51].

The Viewing Wand system (ISG Technologies, Inc., Mississauga, Ontario, Canada) [50], is such system. The Viewing Wand system, an arm-based frameless stereotactic system, uses the Surgicom, a 6 degrees of freedom, articulated, position-sensing arm married to sophisticated three-dimensional (3-D) imaging software. Analog-digital converters transfer the data from the sensors in the three arm joints to an interface processor that calculates the position of the Viewing Wand tip. The tip position is updated 30 times per second. The position data are transferred to an image processor that displays the superposition of the Viewing Wand tip on a 3-D reconstruction and registration of the imaging data. The system is registered at the beginning of the operation by touching the probe tip to fiducial markers affixed to the patient's scalp.

The data before surgery from the imaging study are transferred to magnetic tape and transported to the operating room for reconstruction. Computer-aided medical reconstruction algorithms and Allegro software (ISG Technologies, Inc.) are used to process the imaging data. A number of different points on the surface of the scalp are also entered in the registration, again using the Viewing Wand probe.

Golfinos, has reported that a series of 325 cases in which the Viewing Wand was used

and evaluated for its utility, ease of integration into the standard surgical setup, reliability, and real-world accuracy achieving a useful registration in 310 of 325 cases (95.4%) [50]. Zinreich, et al. found that the mechanical accuracy of the Viewing Wand system, when tested on a plastic model of the skull, was within an average of 1 to 2 mm. Ninety-five percent of errors fell within 3.7 mm. This degree of accuracy is comparable to that of standard frame-based stereotactic system [64]. The Viewing Wand system was used in the Department of Neurosurgery of Great Ormond Street Hospital, to measure the tumour volumes left after surgery. The tumour volume calculations were also derived from the MR images which were obtained before the day of the procedure and about 2 or 3 days after surgery. Volume-acquisition MR imaging was performed with the following parameters for T1-weighted images: 128 256x256 matrix; and contiguous slices of 2.0cm thickness. Injected intravenous gadolinium-DTPA was used to enhance the tumour.

The image data before and after surgery were transferred to our laboratory via standard ftp. We used the 'ANALYZE/AVW' software to register these data and use the multiple display programmes for side-by-side visual comparison of the two scans.

Fig 3.3 is a pair of registered high glioma patient's MR slice before and after surgery. In this case, we can see there is some tumour still left after surgery. Using the image edit program, we can automatically segment the brain tumour volume using the method describe in chapter 4. The volume of eight patients' tumours before and after resection were measured. The result is shown in Table 1.

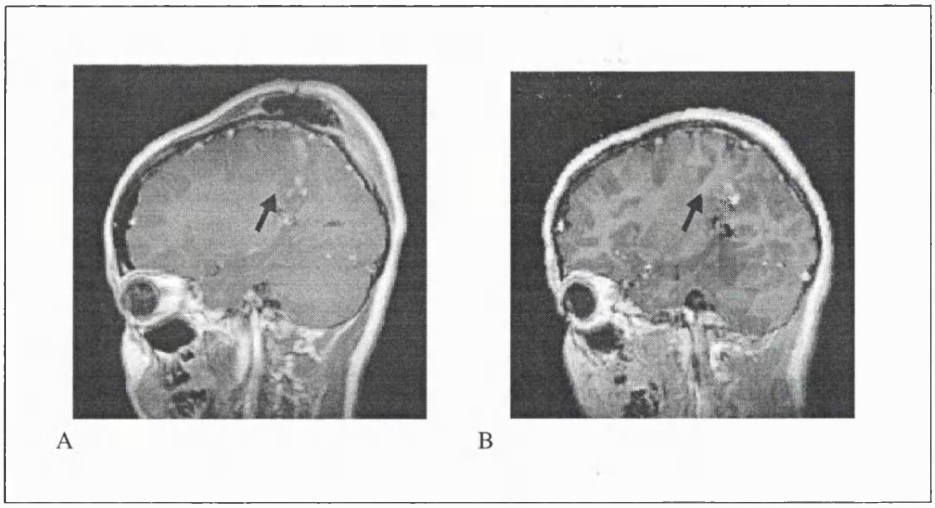

Fig 3.3 *The corresponding brain tumour image before and after surgery. (A) is after surgery and (B) is before surgery .*

In our study, we calculated the volume which should be resected by surgery. 50% of

patients' tumours had been 100% resected. The mean percent of the volume resected was 97.2%. We have been unable to find the report on the volumes measured using the frame stereotactic guiding surgery. But this result reflects the registration accuracy in another way. Our experience with the system confirms comparable accuracy across most of the cases. The worst patient result was for a three year old girl who had medulloblastoma, the errors being mostly due to the depth of the lesion from the surface.

In our experience, the greatest sources of error in the use of this system were attributable to the registration process and to patient movement relative to the Viewing Wand during the operation. In spite of our best efforts, including securely fixing the Viewing Wand arm directly to the Mayfield tongs, movement of the patient's head relative to the Viewing Wand arm occurred and decreased accuracy. Imaging studies, that is MR images, were obtained before the day of the procedure and about 2 or 3 days after surgery. Volume-acquisition MR imaging was performed with the following parameters for T1-weighted images: 128 256x256 matrix; and contiguous slices of 2.0cm thickness. Injected intravenous gadolinium-DTPA was used to enhance the tumour.

Table 1

PN*	Tumour's volume (mm3) per operation	post operation	PR* (%)
1	12,585.00	24.00	99.80
2	35,789.00	0.00	100.00
3	16,234.00	244.00	98.50
4	7,933.00	0.00	100.00
5	4,789.00	0.00	100.00
6	10,654.00	395.00	96.30
7	26,256.00	0.00	100.00
8	23,456.00	1,712.00	92.70

PN* = patient's number PR* = percent of the tumour resect

3.3 Registration for radiotherapy planning

In the treatment of brain tumours, especially low grade gliomas, the major problem of radiotherapy is that a radiation dose sufficient to achieve tumour control will in all likelihood also damage the surrounding healthy tissue. On the other hand lowering the dose may make the therapy ineffective. Many efforts have been made during recent years to minimise the probability of side effects and at the same time improve local tumour control. One way may be stereotactically directed local high dose irradiation. An indispensable prerequisite for this kind of treatment is the accurate delineation of the tumour margins for treatment planning.

The gross tumour volume is defined as the demonstrable macroscopic extent of tumour either palpable, visible, or detectable by conventional radiography, ultrasound, radio-isotope scans, CT or MR scanning. The planning target volume is a geometrical concept and is used for treatment planning. The clinical target volume is a volume of tissue to be irradiated to a specified absorbed dose according to a specific dose time pattern. When planning a patient for treatment, an irradiation technique is developed which provides a maximum and uniform dose to the target volume and minimises both the treatment volume and irradiated volume. The resultant optimised treatment plan will depend strongly on these parameters as well as on the limiting dose to critical normal tissues[6].

Radiotherapy planning is based on the CT image because only CT carries information of the electron density for calculation of dose distributions. Only using CT examination for defining the target volume outline is not enough due to the limitation of the CT imaging of soft tissues. Although most of the hypermetabolic tumours show enhancement on CT, only 50% of the low grade tumours show enhancement, a sign frequently attributed to a high degree of malignancy.

MR continues to show improvement as an imaging modality for the assessment of malignant disease, particularly for sites such as the central nervous system, brain, head and the central nervous system. MR is very useful for defining tumour localisation as well as following tumour response after treatment. However, MR images are subject to geometric distortion and MR parameters are not directly translatable to relative electron densities. Thus MR is a useful tool for providing additional information to the therapy-planning process although it is not capable of replacing CT scanning. As such MR and CT are complementary tools [6].

PET scans are extremely useful for demonstrating tumour uptake of metabolites. As for MR, these nuclear medicine procedures provide additional information that is useful for the delineation of target volume and more accuracy for assessing the regression data of the tumour. The feasibility of using PET to characterise tumours has been demonstrated most extensively for tumours of the brain. Many of the initial PET tomographs were able to image

only the brain.

Several more advantages of PET in brain tumour diagnosis compared to MR have been demonstrated. PET is used in determining the degree of malignancy of a tumour and in determining the prognosis of brain tumour patients. PET is useful in determining the appropriate biopsy site in patients with multiple lesions, large homogeneous lesions, and large heterogeneous lesions. PET is accurate in differentiating recurrent tumour from necrosis in patients who have undergone radiation therapy and chemotherapy. FDG-PET has also been successful in determining the prognosis of patients with brain tumours and PET has also been shown to predict survival in patients with gliomas more accurately than either CT or MR [35].

When these complex imaging modalities do not correlate physicians are restricted to using only subjective methods, normally comparing these corresponding slices by eye and drawing the outline of the tumour and critical organs which can be seen better in one set of images than another. The result is that errors may be made and the treatment will not be the best. It is reported that the clinical target volume was incompletely encompassed in between 25.2 and 17.5% of cases. 955 of deviations of field alignment were less than 10.0 mm (whole brain) with a random error between 4.1 and 7.3 mm. The prescribed dose including deviations of less than 10% was applied in all patients [65]. So delivering the most effective possible homogeneous dose of radiation to an accurately localised target volume in order to produce tumour control with minimal effect on surrounding normal tissues is a very serious issue.

3.3.1 Assessment of tumour outline using registration methoda

In an attempt to achieve effective planning, Lothar [26] described a treatment planning system for stereotactic convergent beam irradiation of deeply localised brain lesions. The therapist can use combinations of CT, MR, and PET data for defining target volume, staging nasopharyngeal carcinoma before external-beam radiation therapy. Cai [52] used a chamfer-matching method for CT and PET lung image registration and fusion. The described registration system has been used to facilitate target definition and treatment planning in radiotherapy. Munle y[53] uses SPECT and PET to help locate the tumour for radiotherapy planning. 11% of the treatment plans were modified by SPECT scans and 48% SPECT datasets were judged to be 'potentially useful' due to the detection of hypoperfused regions of the lungs, but were not used during treatment planning. PET data influenced 34% of the treatment plans examined, and resulted in enlarging portions of the beam aperture (margins) up to 15%. Rosenman [54] reported that using additional MR imaging changed the derived tumour location in the treatment plan by at least 1.5 cm for half of the patients, and up to 3.0 cm for 25% of the patients.

Fig 3.4 is a pair of CT and MR data obtained from the Middlesex Hospital. The patient

suffered from a brain tumour and would undergo the radiotherapy treatment. The tumours were visible in the MR image. In the CT image, we cannot detect the lesion. In order to automatically transfer the tumour outline from MR to CT, we used the software to register MR to CT. The tumour outline was then fused to the CT image using the radiotherapy planning system. The registered MR image was the reference image for the original CT to do the radiotherapy planning.

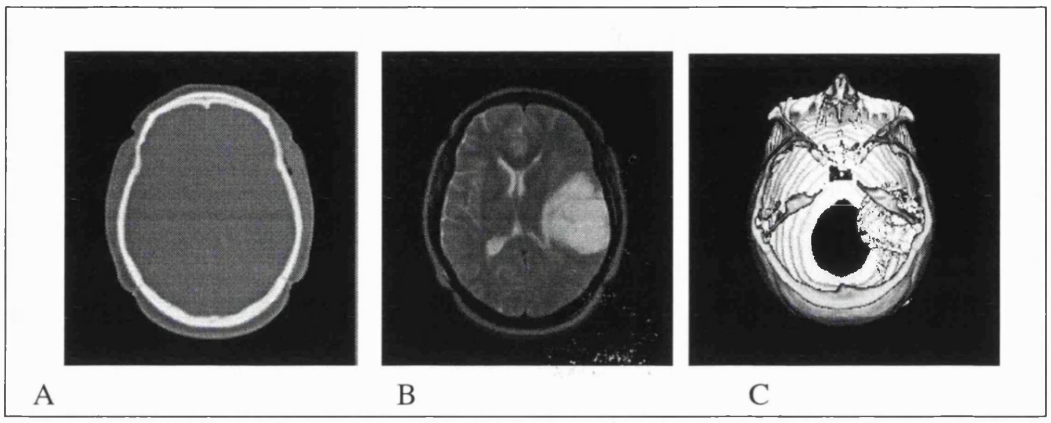

Fig 3.4 *(A) is the CT 2D image, (B) is the registered 2D MR image (C) is the 3D fused image which tumour soft tissue derived from MR and added to CT.*

3.4 Neurology studies using registration methods

The method of registration and subtraction has been used to analyse brain growth of children. This method allows growth and development to be easily identified. Increased growth found in the brain adjacent to the site of neonatal infarction has been the subject of a particularly interesting recent study. This has raised questions about plasticity and regeneration of the brain in infancy [23].

Changes in children may be quite complex, with, for example, contraction changes in the ventricular system due to expansion growth (see Fig.3.5) [23].

Registration and subtraction of MR images has also been used to detect increase and decrease in tumour size following treatment. By using the same method, brain post-operative changes, infarction, Alzheimer disease, schizophrenia, pre-eclampsia, transient ischaemic attack and multiple sclerosis, epilepsy were all analysed through the demonstration of lesions on subtracted images [23].

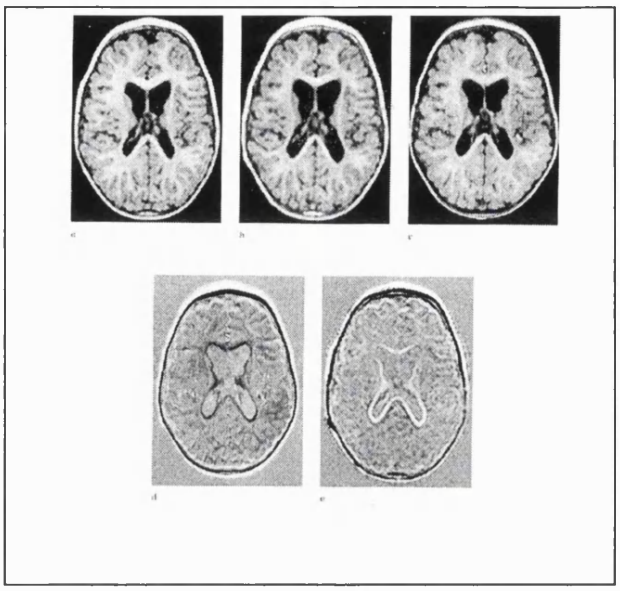

Fig 3.5 *D is the subtraction image (B-A), and E is the subtraction image (C-A).*

We will now consider the relationship in regional cerebral blood flow as measured with perfusion MR and SPECT. After registration rCBF was determined in 10 brain regions relative to the whole slice value. rCBF from pMRI shows good correlation with rCBF from SPECT [55]. There was a significant decrease in rCBF in the frontal, parietal, and temporal regions in the Alzheimer's disease group found by evaluating the effects of various covariants on the distribution pattern of ^{99m}Tc-HMPAO[56]. The brain organisation pathological change in schizophrenia may be expressed at two mutually independent levels of anatomical organisation: global change in a grey matter/ventricular system and supra- regional change in a frontal-temporal system by using registration method.

John [22] uses a paired point method to register MR data to an anatomical atlas followed by image fusion for Alzheimer's disease and epilepsy.

3.5 Other studies

Some research has used registration and fusion for the study of the other diseases. Faber has registered 3-D cardiac images [7]. Automatically detected left ventricular endocardial surfaces were used to determine the best transform between the two sets of surface points, and that transform was applied to the original SPECT image. A fused image created from MR and the transformed SPECT images combined the information in both. The authors tested the method with seven patient studies. Registration reduced the distance between the MR and SPECT left ventricular endocardial surface by 30%, to an average of 2.7 mm. The authors

found that, by using the fused images, perfusion abnormalities could be easily localised and correlated to high-resolution endocardial wall motion and systolic wall thickening.

Gerald and Maguire [12] have fused PET, SPECT, CT, and MR to study younger HIV-positive patients with symptoms of dementia. Bone marrow transplantation has been studied by registering serial MR images of patients with chronic myeloid leukemia [23] The registration of EEG on a patient's cortex surface computed from MR data was reported by Kozinska [57].

Chapter 4 Assessment of the methodology for epilepsy patients' seizure location

Image processing techniques were applied to SPECT brain images to aid in the localisation of epileptic foci. Ictal and interictal SPECT images are collected and these are then registered. Interictal images are subtracted from the ictal image. Registering these subtracted images to MR may improve the clinical diagnosis. Using this technique, we must register ictal and interictal SPECT image first and then normalise these images. After this subtraction is carried out and the threshold range should then be correctly selected to reduce the noise. There are three important issues that influence the accuracy of the lesion location. a) Registration accuracy b) Normalisation accuracy c) Threshold selection. In order to choose the best method for lesion detection, we should make a correct decision through comparing different methods. I will now consider registration, normalisation and thresholding separately below.

4.1 Assessment of the accuracy of different registration methods

An issue which needs to be discussed is the evaluation of registration algorithms as regards accuracy since misregistration gives rise to misleading artefacts. This poses a serious problem in clinical practice, since the best transformation is an unknown. How accurate are the different registration methods and which method is best for transformation between both SPECT and from SPECT to MR for our study? In this chapter, I will review some work which I have done to examine this issue.

4.1.1 Accuracy assessment of registration by visual inspection

It has been mentioned that the accuracy of registration has been assessed qualitatively by visual inspection and the accuracy of registration measurement based on landmarks checked by visual selection. The automatic retrospective registration algorithms can frequently register multi-modalities around 2 mm, but sometimes failed. When using these algorithms routinely in the clinic, methods must be provided for distinguishing between registration solutions that are clinically satisfactory and those that are not. One approach is to rely on a human observer to inspect the registration results and reject images that have been registered with insufficient accuracy. Without firm knowledge of the efficacy of visual assessment, it is highly unlikely

that multi-modal registration will be widely accepted for routine clinical use. Different presentation techniques have been used to evaluate registration accuracy based on visual inspection. E.g., by reformatting the usually transaxial tomographic data to coronal and sagittal slices in which the registration area will be far more obvious. By zooming in on specific structures, a detailed account of all misregistrations can be obtained [30].

The reliability of visual assessment for detecting registration errors is a matter of some controversy. Providing a definitive evaluation of the effectiveness of visual assessment of registration accuracy as a clinical tool will require a large study. Recently Wong et al. reported on five experienced observers' ability to detect misregistration of MR and PET images. This has shown that all observers can detect translational misregistration of greater than 2 mm in the x and y direction, and greater than 3 mm in z direction. Similarly, the observers could always detect rotations of 4^0 or more and could detect a rotation error of 3^0 about any axis at least 80% of the time. The gold standard for this study was an automatic registration algorithm that optimised the mutual information of the joint probability distribution of the two images [67].

By using a method based on fiducial markers fixed to the skull of the patient, as a " gold standard," and by rendering the fiducial markers invisible, Fitzpatrick, et al. [67] were able to perform an evaluation of visual assessment relative to the registration solution obtained using these external fiducial markers. Two experienced observers viewed five pairs of clinical MR and CT brain images in a blind trial, each of which had each been misregistered with respect to the gold standard solution. Fourteen misregistration errors were distributed between 0 and 10 mm with approximate uniformity. For each misregistered image pair each observer estimated the registration error (in millimeters) at each of five locations distribution around the head. These estimated errors were compared with the errors as measured by the gold standard to determine agreement relative to each of the six thresholds, where agreement means that the two errors lie on the same side of the threshold. The effect of error in the gold standard itself is taken into account in the analysis of the assessment methods. No assessment performed well at 1 mm, but all methods performed well at 2 mm and higher.

The result mentioned above are clearly dependent on the modalities they have used, the volume of the patient imaged, the resolution of both modalities, and the MR pulse sequence chosen. They are also influenced by the experience of the observers, the software tools used, the distribution of misregistration errors, and the target points used. Their results do, however, suggest that, the observers were able consistently to detect registration errors around 2 mm.

4.1.2 Evaluation of the accuracy different registration methods

Quantitatively the transformation error can be measured by measuring the difference

between intrinsic and extrinsic points within a data set or by visual assessment. The error has been calculated by averaging the total point's 3D Euclidian distances in most cases. It is difficult to give a more precise estimate of the true registration errors in view of the fact that landmarks chosen have inherent measurement errors. This is because of the limited spatial resolution of current neuroimaging technology, especially the relatively poor resolution of functional images and the limitation of visual assessment. Normally, the total error includes registration and distance calculation errors.

For point based registration, it is reported that the errors was around 1.75 mm for CT to MR [30] and around 3 mm for MR to PET [13]. The range of the error depends on the resolution of both modalities and the number of landmarks used. The accuracy is greater for registration images of higher resolution (eg, MR to MR) than for those with low resolution (eg, MR to SPECT). The more landmarks chosen the more accurate is the registration. The accuracy of image fusion can be assessed both qualitatively and quantitatively using the measurement of the accuracy of independently locating anatomic structures seen on functional images and the anatomic images or using a computer-generated estimate of the mean error vector magnitude between the markers on them.

For the retrospective intermodality brain image registration techniques, Fitzpatrick et al. [31] have compared 12 methods which include: surface matching; mutual information; correction method; minimising a weighted average of the standard deviation algorithms. In their report, the registration results of these different retrospective methods are compared to a gold standard based on screw-mounted extrinsic markers.

The accuracy of fiducial marker system is shown to be approximately 0.5 mm for CT-MR and 1.7 mm for PET-MR. This was estimated by using numerical simulations. Briefly, the simulations are performed as follows: The head is modelled as a hemisphere of radius R = 10cm. In a given simulation they specify the number of fiducials, and the fiducial location error (FLE) in each of two image spaces, where FLE is the root-mean-square error in determining the positions of the fiducials on the surface of the hemisphere and the targets randomly within the hemisphere, perturb the fiducials randomly and independently in each space to simulate FLE, register the perturbed fiducials, and compute FRE and TRE as the distances between the corresponding fiducials and targets, respectively. They performed each simulation 100,000 times for a single target. They repeated the simulations with different values of FLE in each space ranging from 0.2 mm to 2.0mm. The simulations show that the distribution of the ratio TRE/FRE. Then the accuracy of the gold standard can be approximated by multiplying the observed FRE value by this ratio.

The accuracy of different retrospective registrations is measured at multiple "volumes of interest" (VOIs). A VOI is defined in the MR image and its centroid C is determined. Then,

the prospective registration is used to obtain the corresponding point C in the CT or PET using external landmarks. The retrospective registration is then applied to this point, producing C'' in the MR image. Statistics are gathered on the target registration error (TRE), which is the distance between the original point C and its corresponding point C''. They report a detailed, blind evaluation of retrospective techniques based on their target registration error at several landmark locations within the brain. Woods method showed the greatest accuracy for MR and functional image registration, the error was 2.3mm.

For the ictal/interictal SPECT registration, Brinkmann et al. [58] has compared Woods' automated registration algorithm and mutual information correction with surface matching registration. The registration algorithms were compared for (a) three dimensional brain phantom images, (b) an ictal SPECT image from a patient with partial epilepsy matched to itself after modification to simulate changes in the cerebral blood flow pattern and (c) ictal/interictal SPECT images from 15 patients with partial epilepsy. Blinded visual ranking and localisation of the subtraction images derived from the patient images were also performed. Both voxel-based registration methods were more accurate than surface matching registration. Woods' automated image registration algorithm was more accurate than mutual information correlation for the computer-simulated ictal/interictal images and the patient ictal/interictal studies. On the basis of current literature as cited above, the automatic method is more convenient and produces an objective result independent of observer variability. Some observers however clearly perform the registration more accurately than this automatic method. The visual method would therefore still be preferred on a visible section where anatomical points can be reliable marked.

4.1.3 Segmenting the brain boundary and related calculations

Segmentation is the grouping of similar voxels into coherent volumetric structures which can be required for quantitative volumetric analysis, for morphological analysis, or for visualisation purposes. Segmentation techniques can be roughly divided into: statistical classification methods, region growing methods, and edge detection methods [66].

One of the most attractive approaches is the interactive segmentation technique of Höhne and Hanson [66]. It is based on region growing and morphological operations (especially erosion and geodesic dilation, i.e., dilation within a mask volume), and requires a user defined seed point and a threshold range. For the analysis of medical volume data, I have used the Höhne approach incorporated into 'ANALYZE/AVW' for segmentation. The method proved to be very practical for reasons of speed, simplicity, and intuitiveness. The technique first extracts a base volume from a dataset using operator defined thresholds, thereby encapsulating the required object. A series of erosions is applied to remove undesirable linkages with other

structures. Subsequent connection to a user defined seed point and geodesic dilation results in a segmentation of the required object. A considerable part of the process can be automated, but the process still requires a user selected seed point and a threshold range.

The selection of a point and choice of the threshold range is crucial to the success of the process. According to our experience, using the procedure as below is quite efficient.

The segmentation method first selects a starting threshold value Tstart and a seed point. Tstart is determined by calculating the second peak in the histogram of grey values of the MR data (the first and highest peak of the histogram represents background voxels). A spherical search from the middle of the dataset is initiated and the first encountered point in the seed volume is marked as the seed point. The threshold range detection has Tstart and the seed point as input to first detect the lower threshold or Tlow and then the upper threshold Tup in a similar way. To detect Tlow or Tup the threshold setting decreases or increase from Tstart.

Normally, the peak Tlow or Tup is detected at the steepest gradient of the histogram. A sharp increase in the number of growing steps signals the inclusion of a new segment through a linkage between two structures; the previous threshold setting is selected as Tlow and the Tup is detected by going upward from Tstart to meet another sharp increase. The parameters of segmentation for the region growing, erosion and dilation processes were set to two erosions and three (number of erosions plus one) geodesic dilations using a 6-voxel structuring element. This was based on information from the 'ANALYZE/AVW' reference manual and our experience with segmentation procedures. The final segmentation is performed by applying the seed point and the threshold region [Tlow-Tup] for segmentation of the brain. The accuracy of this method in separating MR brain voxels was greater than 97% in most of the cases [42].

This method has been tested using a phantom. The phantom is a cylinder which contains three small containers. One for gases, one for solids and one for liquids. The phantom was filled with gadolinium for an MR study in the liquid container. At Middlesex Hospital, the phantom has been scanned by MR. The MR scans have been acquired on a SIEMENS Open MR imager. Standard T1-weighted, images were displayed as 128 256x256 images. The pixel size was 1x1x4 mm. The 3-D phantom data was transferred to a SUNSparc workstation which is installed in our department. The image segmentation processing and calculation used was the method mentioned above. AVW/Analyze software was used for imaging processing.

Figure 4.1.B shows the histogram of the circular area presented in Figure 4.1.A. which is the phantom. We wanted to segment the volume which lies inside the circular region. The second peak of this case is at 170. The Tlow and Thigh are 158 and 183. Fig 4.2 shows the result for three containers after segmentation. The volumes of the three containers were calculated. The results are shown in Table 2. The accuracy of the segmentation of these three

containers are 99.56%, 99.96% and 99%.

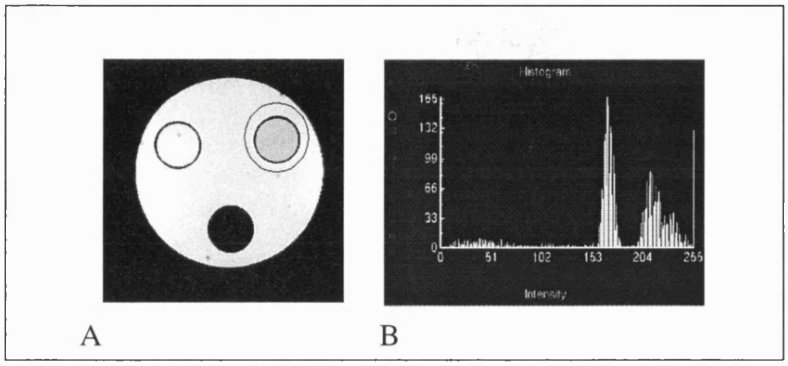

Fig 4.1 *A is the MR phantom image, B is the histogram of the circular area presented in Fig 4.1 A.*

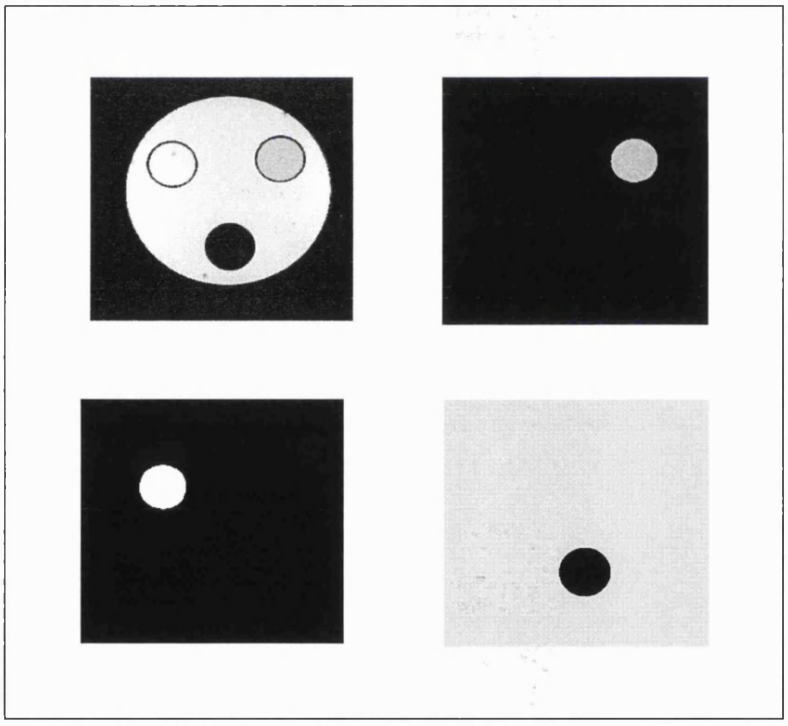

Fig 4.2 *shows the result for three containers after segmentation.*

Table 2

	Contains' name	Volumes(cm^3)
Real phantom's volume	solid	4000
	gas	3180
	liquid	3180
Volume calculation	solid	4040
	gas	3194
	liquid	3318

For children aged under 2.5 years, the volume of the brain is continuously increasing with age [32]. Normally, SPECT ictal and interictal study times were separated by one week. But sometimes images of the brain taken at different times during growth were studied. In the Table 3, we can see that the time between the ictal/interictal scans for patient 2 was 8 months and the volume increased 10.1% and patient 6's volume increased by 8.8% during 7 months. In these cases, non-rigid transformation was selected for correcting the size and shape change. The scaling in size between ictal/interictal SPECT registrations and subtraction is quite important. Non-uniform volume image subtraction may lead to the appearance of extra artifacts.

Table 3

Patient number	Age	The scanning days between ictal and interictal	Volume change
2	1.5	7months and 3 days	10.1%
6	1.1	6months and 13 days	8.8%

We used the semi-automatic segmentation method mentioned above to segment and calculate the perfusion volume of ictal/interictal SPECT images and the brain images from MR. The brain volume calculation was based on the segmented brain boundary.

4.1.4 Comparing rigid and non-rigid registration for the brain shape changes

For multiple images the patient's soft tissue structures may well demonstrate a shape

change, hence a deformation will be needed to accurately register the scans together. Here there is quite often a patient shape change between scans and a non-rigid approach is reported. For example, for estimating correct breast movement between two scans, movement of the chest is represented as a rigid body while the remainder smoothly deforms. Non-rigid registration is always used for mapping real patient brain data to the atlas.

Woods has tested rigid and non-rigid registration using different transformation models for different size of brain studies [59]. The brains in the MR images of 22 persons were warped individually to the anatomical atlas using different transformation algorithms. Each spatial transformation model and method was assessed by using the resulting transformations to map the traced landmarks from all 22 subjects into a single volume in the space defined by the average brain MR atlas so that the overlap of the homologous landmarks could be evaluated both visually and quantitatively. Since the cortical landmarks consisted of sets of voxel locations defining homologous structures, rather than of individual point landmarks having one-to-one correspondences, quantitative comparisons could not be based on errors in the locations of individual homologous points. Instead, for a given landmark voxel in one subject, the distances to each of the voxels comprising the corresponding landmark in a second subject were calculated, and the shortest of these distances was defined as the distance function for that landmark voxel with respect to that second subject. This resulted in 21 different distance functions for each landmark voxel of a given subject. These 21 distance functions were then averaged to produce a mean distance function for that particular landmark voxel in that particular subject. Over 90,000 mean distance functions were computed for each registration strategy, corresponding to several hundred voxels per cortical landmark for each of five landmarks in both hemispheres of 22 subjects. The cumulative distribution of these mean distance functions for each registration strategy then displayed graphically using S-plus. Non-linear models lead to further improvements in the match of the shape of the brain to that of the target.

The lack of gold standard transformation makes evaluation of non-rigid registration accuracy difficult. For nonlinear spatial transformation models, it is especially importance that the assessment of accuracy not rely solely on simple visual inspection of resampled images. High order non-linear transformations may be able to create and destroy sulci and gyri to make the resampled image look similar to the target. The resulting images may suggest excellent registration, and only discrepancies in the locations of homologous anatomic landmarks identified in the original images and mapped into the target atlas will reveal whether the procedure has failed to achieve its true objective. The results in Woods' paper show that the relatively low order nonlinear transformations in the mapping of homologous anatomic landmarks to consistent location.

Even if the calculated registration transformation is perfect, a scaling error of 2% can result in registration error up to 4 mm across a 200-mm FOV [59]. Rigid and non-rigid methods have been compared by scaling and transforming a simple MR brain image and then by using one of the methods to register this back to the original image. The test data were a set of MR T1 weighted brain image acquisitions from a 1.5T Siemens intended to show good grey/white matter delineation. The original data was sampled at 256x256x128 giving a voxel size of 0.965 x 0.965 x1.0 (mm). First, we manually edited the data to a smaller region enclosing the brain. This region was scaled down in size by 5% and 10% producing two new volumes. These volumes were then rotated by 30 degrees about the principal axes and then translated by 10 mm in three-dimensions.

Wood's software using rigid and non-rigid transformation models which is installed in the computers in our department were applied to register the scaled and translated data set to the original one. Optimisation using the Wood's non-rigid (second order non-linear model) measure provides a finer transformation parameter step size for the children for whom the volume of brain has increased.

Fig 4.3 shows the contour of the MR data derived from the result obtained using these three different methods and fused to the original data. A, B and C are using Wood's rigid method and D, E, F are using Wood's non-rigid method. The first raw image has no size change, the second image is for size reducing 5% and the third image is for a size reduction of 10%. From this picture we can see that the contours using Wood's non-rigid method are the most similar compared with the original image for volume change. Using the rigid transformation the volume was not restored to the original volume, but it was restored using non-rigid registration.

From the result of applying Woods' algorithms, we conclude that using low-order nonlinear registration transformation is more suitable for cases of volume change. For our test we only pay attention to the volume scaling change. Brain growth is more complex and non-uniform. The perfusion images at different times should be different. There exist some errors using this technique that cannot be measured due to the real perfusion image being unknown. Because the major difference in the ictal/interictal SPECT localise on the small lesions, using this kind of model would be more reliable in practice.

4.2 Normalisation scheme

For determining the difference between ictal and interictal conditions of the brain in epilepsy patients from image data, a normalisation process must be carried out. This is because the SPECT images represent the distribution of radiopharmaceutical in the brain, which is an indirect measure of perfusion. Ideally, an area of the brain not associated with the

seizure focus would contain the same distribution of the radiopharmaceutical in both the ictal and interictal state, and the seizure focus would contain an elevated concentration of radiopharmaceutical, which would highlight its location. Due to the extraneous influences, normal brain areas contain different concentrations of radiopharmaceutical in the ictal and interictal images. The radiopharmaceutical concentration is influenced by:

- The total injected dose, which is not identical for both imaging sessions;
- The acquisition time when the scanning procedure is different, since the radiopharmaceutical undergoes a chemical decay process which is significant over minutes;
- The general condition of the patient and uptake characteristics of the brain not being consistent since imaging sessions are conducted on separate days .

For the normalisation, all the reports are based on the mean cerebral pixel intensity of these data [36] [37]. The appropriateness of this linear normalisation was studied by comparing the pixel intensity distributions [60]. The pixel intensity distribution for both six normalised phantom, and 10 paired normalised patient studies, were closely matched to each other except for the extreme values, which in clinical situations are likely represent regions of ictal activation or depression. If the co-registration and normalisation are correct, the distribution of the subtraction intensities should approximate to a normal distribution symmetrically centred around zero for those regions in which the rCBF is not significantly changed by the seizure activity. This spread represents the inherent noise between the two images. If the images are not well normalised, the median value of this distribution will be greater (or less) than zero as a result of the 'normalised' ictal image being relatively more (or less) intense than the 'normalised' interictal image. The results showed that the subtraction image intensity distributions were symmetrically centred on zero for all values up to at least within the 5th to 95th percentile range, confirming good normalisation for the 'non-activated' pixels. Also, a linear relationship demonstrated that this method produces accurate SPECT to SPECT co-registration, and appropriate SPECT normalisation, thereby allowing a valid ictal subtraction image to be derived. In contrast, the range of the extreme values was much greater, positively skewed, and in the phantom subtractions showed much more variability.

original data

Wood's rigid

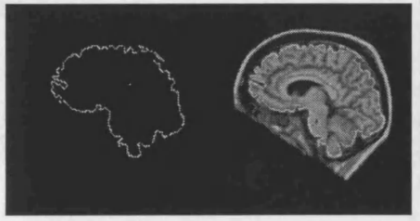

A(no size change)

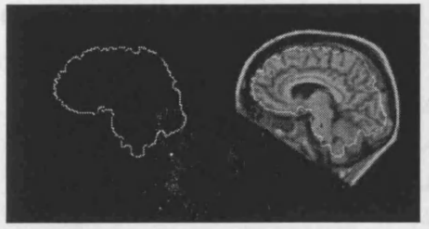

B(size reduced 5%)

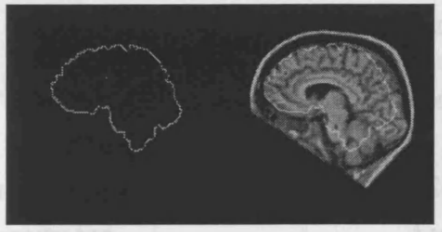

C(size reduced 10%)

Wood's non-rigid

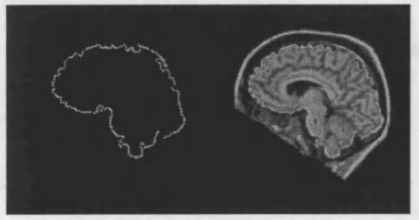

D(no size change)

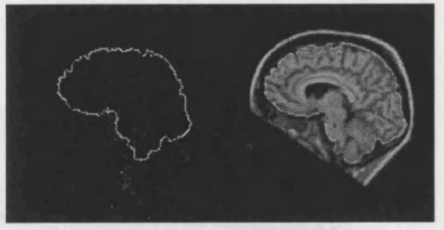

E(size reduced 5%)

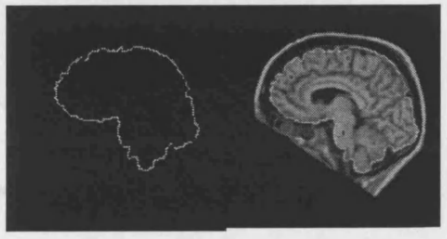

F(size reduced 10%)

Fig 4.3. Notice in each case the degree of complinance of the contour with the brain image. Contour of brain derived after registration using wood's rigid and wood's non-rigid algorithm. The contours superimposed on original MR image.

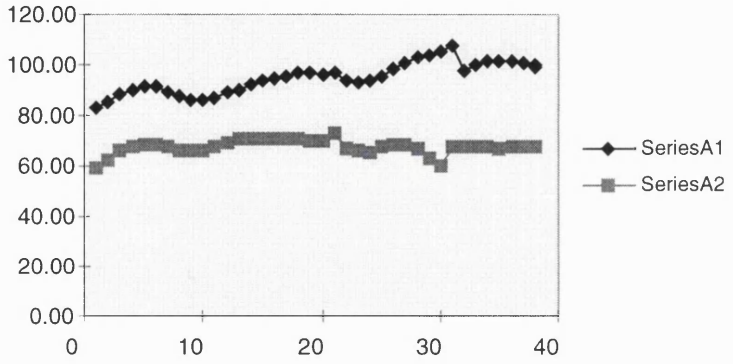

A. Series A1 is the mean intensity for patient 2 ictal image different slices. SeriesA2 is the mean intensity for patient 2 interictal image corresponding to these slices

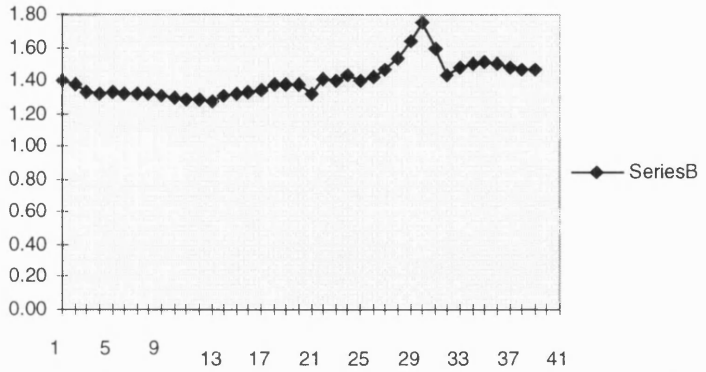

B. Series B is the percentage change between ictal and interictal at for patient 2

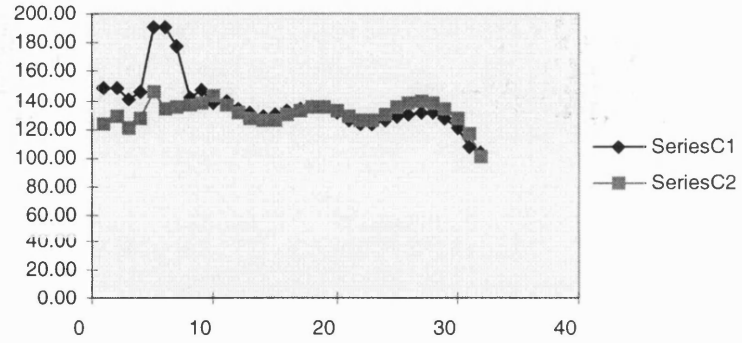

C. Series C1 is the mean intensity for patient 3 ictal image at different slices. Series C2 is the mean intensity for patient 3 interictal image corresponding to these slices

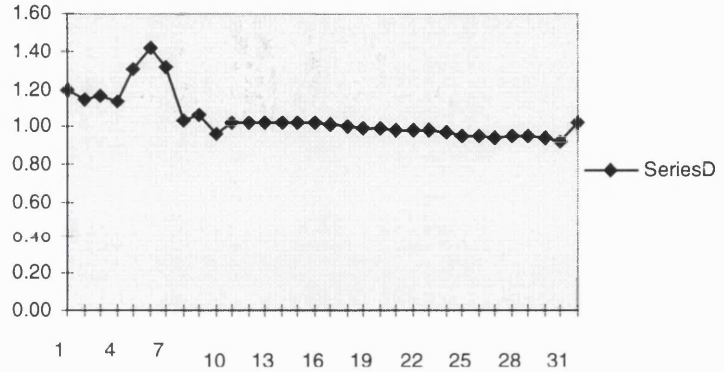

D. Series D is the percentage change between ictal and interictal for patient 3

Fig 4.4

The normalisation according to the mean cerebral pixel intensity is based on the hypothesis that the regions of increased blood flow during partial seizures are relatively small compared to the total brain volume, and are at least partially balanced by other brain areas with a decreased perfusion. How should we normalise the ictal and interictal images for the children in which multiple lesions are often present? For these patients, we used another method based on the mean pixel intensity. According to our experiences normalising total counts of pixels based on the pixels without lesion activity is better than normalising total counts in the brain as described above.

Fig 4.4 shows the result of two patients (patient 2 and patient 3) showing the mean intensity of the corresponding ictal and interictal slices and the percentage of these slices. The slices which corresponding to the lesion positions are quite different from others in all the cases. So we can conclude that the better way to normalise the ictal/interictal images is based on total counts excluding the lesions in these cases. This is because the areas of the brain associated with seizure focus should vary strongly between interictal and ictal states but usually influence the uptake of the brain and measured uptake ratio especially when the lesion is large.

In order to confirm our conclusion we carried out SPECT normalisation and image subtraction for the 11 patients. The results of the analysis of the distribution of the pixel intensities in the subtraction images for these patients are summarised in Table 4 and Figure 4.5 and Figure 4.6. in all cases for pixels within at least the -2SD - +2SD percentile range, the distribution was symmetrically centred around the zero value.

4.3 Threshold selection for subtraction image

After registration and normalisation of the ictal and interictal SPECT images, we subtract one image from the other where the value for each pixel represents the intensity difference between the two data sets. From the Figures 5.1, 5.2 and 5.3 we can see that the subtraction images (C) showed a distribution of bright pixels all over the image. It is difficult to find the foci of lesions. There are several factors influencing the lesion intensity. These may be due to registration error, normalisation error and different noise distributions between two scans. Assume the error of normalisation and registration are small enough. Then the subtraction image will include the difference noise and lesion distributions.

4.3.1 Different threshold selection schemes - a general review

The significance of multiple foci of hyperfusion present in patients is the question we now wish to address. Depending more or less on the threshold selected, foci can be revealed on the subtraction images to display only the ictal increase in intensity that was significantly

greater than that of the background. In order to disclose most perfusion abnormalities, different people use different strategies. It is reported that three methods have been proposed to quantify subtraction images.

Zubal et al. [36] has used a method which calculates the percentage change between the subtracted and interictal images. Ictal and interictal cerebral perfusion SPECT images were acquired from 12 epilepsy patients after injection of 20 mci ^{99m}Tc-HMPAO. Once the transverse slices have been realised and normalised for proper registration, two separate difference images are computed. On a pixel-per-pixel basis, the difference in pixel values is divided by the pixel value from the interictal scan and then is multiplied by 100. This new value is written into one of two functional image matrices. Positive values are written into a positive difference image, and negative values are written into a separate negative difference image. In this way increase and decrease of blood perfusion can be viewed separately on a slice per slice basis. Since the values stored in the difference images numerically correspond to the percent change in perfusion, regions of interest can be drawn on the difference images in order to quantify the perfusion changes. Region of interesting analysis indicates that the brightest areas noted in the difference images exhibit perfusion changes of 50% or larger. In many cases, these areas correspond to primary seizure sites as confirmed by depth electrodes and can be interpreted as areas which exhibit the largest change in perfusion. In this method, all the different areas were represent in the images. But we need to calculate the different areas and selected the highest areas which were usually greater than 50% increase corresponding to the lesion. In some cases there were other areas lower than this figure. There were some drawbacks that first we could not directly locate the lesion, and secondly that the method was labour-intensive. Another important issue that defined accuracy of this figure was that they only had data for four successful surgical outcome patients. If there are more lesion locations in the brain (especially for the case of children), one question is how many location we should chose and what are the percent change figures for these.

Pierre, et al. [61] uses a threshold of 40% of the maximum of the smoothed subtraction images for children. Twenty-seven children with partial epilepsy (aged 3 months to 18 years) underwent ictal ethylcysteinate dimer (ECD) SPECT (20mCi/1.73m2) combined with video-electroencephalography (EEG) and interictal ECD SPECT followed 2 days later by three-dimensional MR scanning. For each subtraction image, three thresholds (20% 30% and 40%) were examined, and the one that disclosed the most perfusion abnormalities (most often 40%) was selected for further analysis. Overlay images allowed the detection of at least one hyperperfused focus in 93% of the children, compared with 74% using ictal and interictal scans separately. It is not reported how accurate the use of this method is. In his study those with the highest level of perfusion increase have been shown to be the closest to the

epileptogenic focus and that the multiple foci were observed and needed to be confirmed by intracranial EEG data. Using this method directly also has the potential to confuse between the lesion location and the propagation of the seizure or noise. O'Brien [37] used a method which selected the threshold range above 2SD to localise the lesion with normalisation based on total counts in the brain for the adult. This was done to minimise the influence of random noise by displaying only those pixels with an ictal increase in intensity that was significantly greater than that of the background. It should be noted that, even if there is not a true region of focal increased intensity on the ictal SPECT, approximately 2.5% of the pixels in the subtraction images will exceed the 2SD threshold by chance alone. However, in such a case, the "significantly" increased pixels should be randomly distributed throughout the image and not clustered in a focus. A subtraction image was therefore considered to be localising when the cerebral cortical pixels with the largest ictal/interictal difference were clustered in a localised area. They studied 51 consecutive intractable partial epilepsy patients who had interictal and ictal scans. They conclude that using this method improves the sensitivity and the specificity of SPECT in localising the seizure focus for epilepsy surgery. Using this method, it is easier to detect significant changes between ictal/interictal images. On the other hand, it is possible that a focus with only a small ictal increase in intensity may be missed with this method if the increase is less that 2SD of the noise between the images. This may be more frequent in the cases with the later injection time.

In comparing the different approaches to choosing a suitable threshold for the detection of hyperfusion in different images, it should be note that the use of 2SD's is best in terms of the theory of a normal distribution of noise. If this model is correct, there would seem to be little significance in selecting a threshold based on a percentage increase in intensity.

4.3.2 Estimating threshold selection method using Gaussian model for our study

It has been observed that most nuclei existing in nature are stable and have high binding energies per nucleon. On the other hand, certain nuclei have lower binding energies per nucleon and are not stable. These nuclei transform themselves randomly and spontaneously to form more stable configuration. These transformation can result in the emission of particles or photons and energy from the nuclei. Measurements of decay rate will fluctuate about the average decay rate since radioactive decay is statistical in nature and based on Poisson statistics. At higher count rates the result is a Gaussian curve. The major noise in an image is due to the statistical fluctuations in the number of γ-ray photons detected per unit area and the properties of the image receptor and display system.

The relationship between the image function $m(x)$ and the object function m(x) is

governed by the point spread function h(x) and noise function e(.) of the imaging system. The relationship can generally be modelled by:

$$m(x) = \int h(x-u)m(x)du + em(x, m(x)). \qquad (4.1)$$

In SPECT imaging the measurements making up an image effectively represent the radioisotope density due to tracer uptake at a given location. The inherent detected noise has an approximately Gaussian distribution. Due to the limitations of the technique there is no method to separate the noise from the image. So there are only the estimation methods to best locate the lesion as mentioned above. Selecting a threshold which is greater than two standard deviations (SD) displaying only pixels with values greater than 2SDs above zero to show the lesion seems more reliably and direct. We used the Gaussian model to fit eleven patients' subtraction images for our study.

Eleven patients with intractable partial seizures received ictal and interictal SPECT scans after injections of approximately 740Mbq of ^{99m}Tc-HMPAO performed at the Great Ormond Street Hospitial. After registration and normalization, the subtraction images were obtained. The histogram of these images were matched with the Gaussian model using Excel software. The results of the analysis of the distribution of the pixel intensities in the subtraction images for the patient studies are summarised in Figures 4.5, 4.6 and Table 4. Figures 4.5 and 4.6 show the histogram for these eleven patients of subtraction images and the corresponding Gaussian model. In all cases, for pixels within at least the -2SD to +2SD range, the distribution was symmetrically centred around the zero value, and virtually identical for all eleven patients. In contrast, the range of the extreme values was much greater in the patients subtraction images and showed much more variability. The results of chi-squared statistical analyse are showed in Table 4. $\chi 2$ has been derived by using the actual data and the Gaussian model over the centre region of the subtraction image histogram. The centre region is defined as area between ⇧2SD for the mean. Given in the Table 4 are the $\chi 2$ values and their statistical significance. For all except one case, $P< 0.05$ showing that there is no significant difference between the prediction of the model and the subtraction image histogram. The table also shows the $\chi 2$ values for the region beyond +2SD where all values obtained show a significant difference ($P<0.01$) between the model and subtraction image histogram. We note that for one patient (patient one), the $\chi 2$ test indicate a marginal rejection of the null hypothesis at $P<0.05$. This may possibly indicate that the Gaussian model does not describe the distribution as well in the case. This may due to the noise of a non-random nature around zero.

Two additional factors that need to be considered are the relationship between measured

differences in intensity between the images and the true differences in ^{99m}Tc activity, and the relationship between changes in rCBF and the brain uptake of the radiotracer. The relationship between measured image intensity and brain ^{99m}Tc activity may be affected by filters applied to the raw image in the reconstruction process. However, we have demonstrated that, with our methods, a close to linear relationship exists for the mean value and for the central range values.

4.4 Conclusions

In this chapter, we have described the technical aspects of our method for deriving the final subtraction image. The SPECT to SPECT co-registration method was shown to produce reliable results based on the Woods' method. We also showed that the normalisation of the ictal and interictal images according to their mean cerebral pixel intensity excepting the lesion provides appropriate normalisation in patient studies. We also confirmed there were more significant changes in the areas greater than 2SD from the mean. These findings suggest that meaningful subtraction images can be derived.

Table 4

patient number	Central range χ2 number	Statistical significance (20 points)	Greater than +2SD range χ2 number	Statistical significance(20 points)
1	31.49	P<0.05	157.61	S (P<0.01)
2	5.50	NS	151.44	S (P<0.01)
3	9.51	NS	124.26	S (P<0.01)
4	12.52	NS	159.08	S (P<0.01)
5	15.53	NS	109.23	S (P<0.01)
6	10.54	NS	397.28	S (P<0.01)
7	1.07	NS	47.61	S (P<0.01)
8	10.05	NS	413.48	S (P<0.01)
9	10.55	NS	173.84	S (P<0.01)
10	9.56	NS	157.16	S (P<0.01)
11	8.12	NS	31.69	S (P<0.01)

NS: not significant S: significant

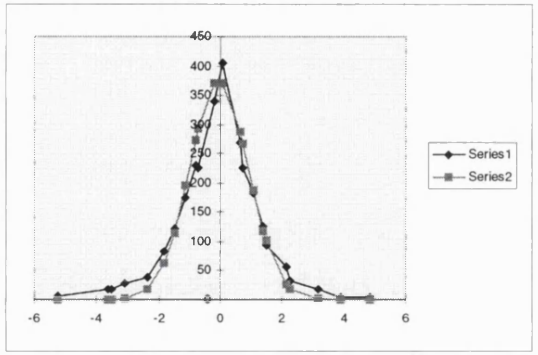

A (patient 1)

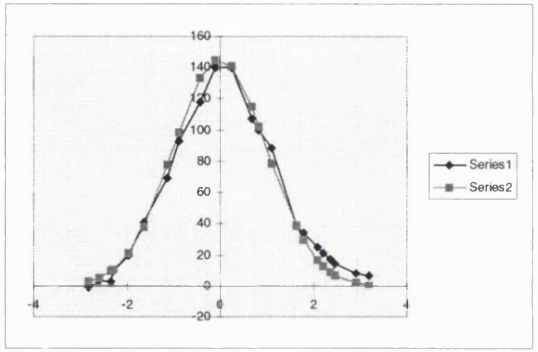

B (patient 2)

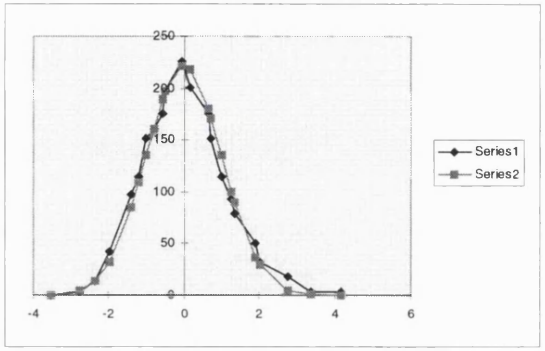

C (patient 3)

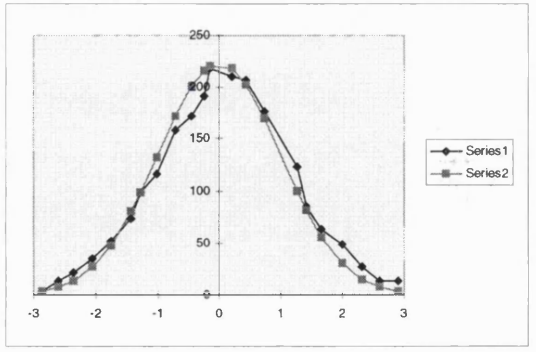

D (patient 4)

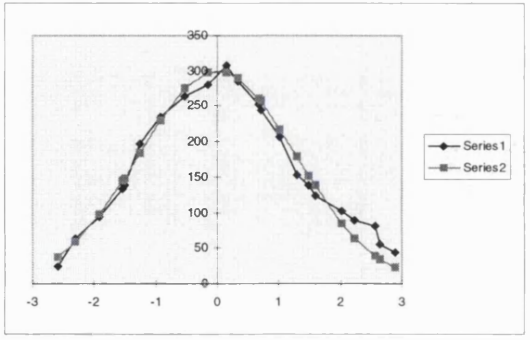

E (patient 5)

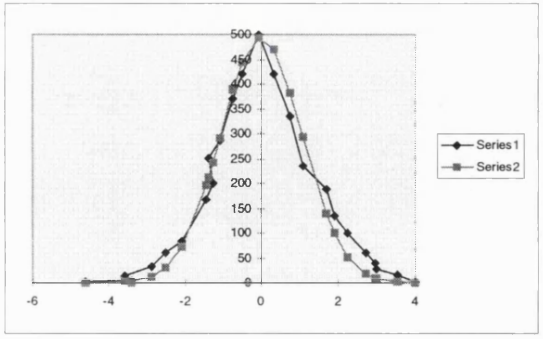

F (patient 6)

Fig 4.5 Comparison of Gaussian distribution model and grey histogram of subtraction image. Grey squares is model, black diamond is data.

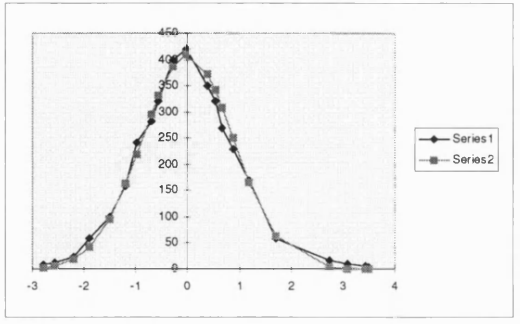

A (patient 7)

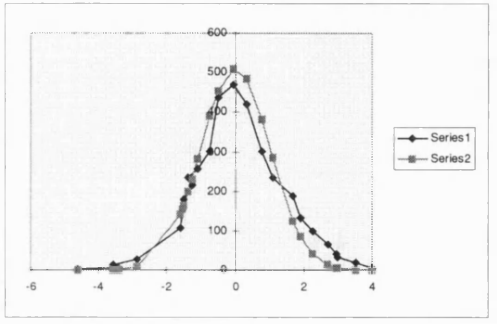

B (patient 8)

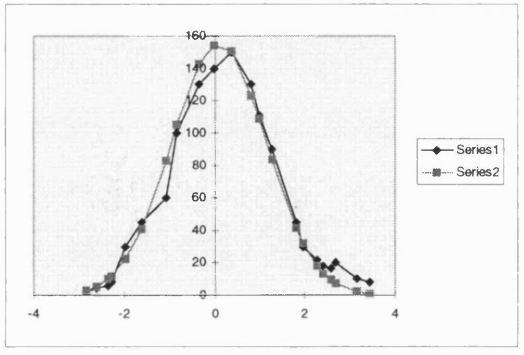

C (patient 9)

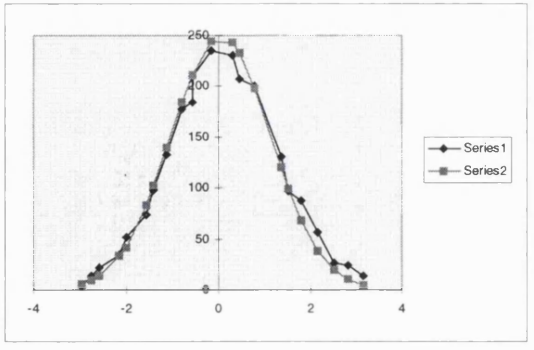

D (patient 10)

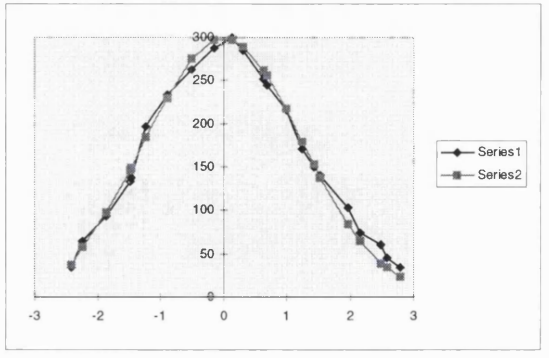

E (patient 11)

Fig 4.6 Comparsion of Gaussian distribution model and grey histogram of subtraction image. Grey squares is model, black diamond is data.

Chapter 5
Registered ictal and interictal SPECT images for helping diagnose epilepsy in children - A validation study

The interictal images were transformed and normalised to the ictal images and then subtracted from them to create an image where the value for each pixel represents the intensity difference between the two data sets. The standard deviation (SD) of the distribution of the subtraction pixel intensities was calculated, and the subtraction image thresholded to display only pixels with values greater than 2SDs above zero. These were fused with the MR images. The result is compared with the EEG, visual diagnosis and surgical outcome. This study indicates that the technique may enhance the ability to localise epileptic seizure foci. The study was based on eleven children who were suffering from epilepsy at Great Ormond Street Hospital.

5.1 Background

5.1.1 Epidemiology of epilepsy in children

Epilepsy is one of the most prevalent serious neurological disorders. It is estimated that 1 in 20 of the population will have an epileptic seizure at some point in their lives and, at a conservative estimate, 1 in 200 will have epilepsy. Seizures are the commonest problem encountered in paediatric neurology. It has been estimated that 75% of cases of epilepsy have their onset before 20 years of age. From data obtained through the National Child Development Study in Great Britain, Ross and Peckham found a prevalence of epilepsy of 4.1/1000 in children followed to the 11th birthday [34].

5.1.2 The role of SPECT in epilepsy for children

Functional brain imaging requires radiotracers that cross the blood brain barrier, distribute proportionally to regional cerebral blood flow, and remain fixed in the brain, estimates of regional cerebral blood flow (rCBF) are based on the microsphere model, which assumes that:

1.) the radiotracer is freely diffusible from the blood pool, 2.) it is completely extracted from the blood into the blood brain barrier, and 3.) it remains fixed within the brain without redistribution.

It is believed that these compounds gain entry to diseased brain tissue through alteration in the blood-brain barrier. However the mechanism by how these agents are retained in diseased tissue is uncertain. It is believed that pathological processes within the brain contain more extracellular water than most normal brain tissue. Therefore, the water-soluble chelate that gives entry into the lesion will equilibrate with this extracellular water, thereby showing increased activity in the area of the lesion. The radio-active tracer used in epilepsy studies is ^{99m}Tc-HMPAO which is a lipid-soluble macrocyclic amine. Once it crosses the blood brain barrier, ^{99m}Tc-HMPAO is converted into a hydrophilic compound in the presence of intracellular glutathione and is trapped, with slow blood clearance.

SPECT is a valuable clinical tool in the management of patients with medically resistant partial epilepsy who are under evaluation for surgical treatment. The value of SPECT for localisation has been firmly established for patients with temporal lobe epilepsy and ictal SPECT is also frequently used to guide intracranial grid electrode placement when seizures are of extratemporal lobe origin.

Between seizures, the interictal period, cerebral blood flow (CBF) and metabolism may be normal or reduced. A reduction in the temporal lobe containing the seizure focus is frequently present in patients with temporal lobe epilepsy (TLE), while interictal regional abnormalities are uncommon in other forms of epilepsy in the absence of a structural abnormality. An interictal SPECT study is also important for accurate interpretation of ictal studies, especially when an extratemporal focus is suspected [35]. The success of interictal SPECT in lateralizing temporal lobe epilepsy onset is quite variable, with estimates of its sensitivity ranging from 36% to 96% and specificity ranging from 36% to 94% [37].

Regional cerebral blood flow (rCBF) to the epileptic focus increases by up to 300% during a seizure. Ictal studies are obtained by injecting ^{99m}Tc-HMPAO during the seizure or within approximately 30 seconds of its completion. Many approaches to ictal injection have been tried. Those centres that are able to routinely obtain ictal injection within 90 seconds of seizure onset usually have an EEG technologist to give the injection stationed near the monitoring rooms and a nurse, relative or volunteer constantly with the patient so the onset of seizures can be rapidly detected. Over 200 patients with unilateral temporal lobe epilepsy proven by ictal EEG, MR and other ancillary investigations or by seizure-free surgical outcome have been studied with ictal SPECT [35]. Ictal SPECT has been shown to have a higher success in lateralising seizure onset in patients with well-established TLE, with a reported sensitivity of 75% to 97% and reported specificity ranging from 71% to 100% [37]

for adults.

The first reports of ictal SPECT in children are promising but still too few for comparison with other methods. Non-invasive identification of the epileptogenic focus is of particular importance for children, but is usually more difficult to achieve than in adults. The reasons for this are:

- The semiology of partial seizures in children is difficult to assess, and the anatomo-clinical relationships are not as clearly established as in adults;
- The seizure onset is often apparently generalised or lateralized to a whole hemisphere and cannot contribute to localising the focus;
- Most epilepsies are extratempoal in origin at this age, resulting in a panel of frontal, parietal or occipital foci, which are known to be more difficult to localise than the temporal ones;

5.1.3 The role of MR in epilepsy for children

A higher proportion (30%) of patients do not exhibit any lesion on MR. A lesion is a useful guide for localising the epileptogenic focus, although the epileptogenic zone cannot be superimposed on the lesion, and resecting the latter may fail to cure the epilepsy [25].

Magnetic resonance imaging hippocampal atrophy can be identified on the side of the seizure focus in up to 75% of patients with TLE. Reduced hippocampal volume on MR has been shown to predict good seizure control and a low risk of developing short-term memory difficulties after operation. A postoperative MR study has shown an association between seizure reduction and the extent of mesiobasal temporal lobe resection. MR will identify small tumours and may show neuronal migration abnormalities and focal cortical dysplasia in some patients with intractable epilepsy [35]. But in some case, seizure focus cannot be detected by MR.

5.1.4 The role of EEG

Electroencephalography remains the most important investigation for seizure focus localisation. All surgical centres employ interictal EEG and video-EEG recording of seizure as the basis of localisation. Ictal EEG from scalp electrodes dose not permit confident localisation in 40% of patients with TLE if used in isolation. However, in most patients confident localisation can be achieved when ictal scalp EEG is supported by ictal clinical features and ancillary investigations such as MR, SPECT. In patients in whom investigations are contradictory, intracranial ictal EEG studies are performed. Serious complications including intracerebral hemorrhage and infection, although rare, have occurred following

insertion of intracranial electrodes so non-invasive localisation should always be attempted first.

5.1.5 The role of surgery in epileptic children

Most medically resistant or refractory patients have partial (focal) seizures and many can be helped with surgery provided the seizure focus can be accurately located.

Many patients with refractory partial seizures can be rendered seizure free with surgery. Experienced epilepsy surgery centres obtain a 70% or greater seizure-free outcome with anterior temporal lobectomy with minimal associated morbidity. Resection of extratemporal foci is less effective and more hazardous than temporal lobectomy, with only 40-50% rendered seizure free. Although recent advances have been made with new antiepilepsy medications, only 5% of patients with refractory partial seizures can be rendered seizure free by the addition of a new antiepileptic drug [35]. Consequently, surgery remains an important treatment option.

5.2 Materials and methods

5.2.1 Patients and injection procedure

Eleven patients with intractable partial seizures received ictal and interictal SPECT scans after injections of approximately 740Mbq of ^{99m}Tc-HMPAO performed at the Great Ormond Street Hospitial, between December of 1996 and January of 1999. The ages of the patients were between one and thirteen. Seizure onset was considered to be the time of earliest indication of abnormal movements, behaviour, or impaired awareness. The end of a seizure was the time when ictal movements or behaviour ceased. For ictal studies, patients received injections during EEG documented seizures which performed by specifically trained EEG technicians. Interictal injections of ^{99m}Tc-HMPOA were performed in ambient room lighting, with the patients' eyes open and ears unplugged, and when the patients had no documented seizure activity in the previous 24 hour period. Images of interictal and ictal studies were acquired using the same scanner and identical protocol, within 90 min of injection.

5.2.2 Imaging method

A dual-headed gamma camera system (Helix system) was employed. The data were acquired in a 128x128 matrix over 360^0 with 120 views obtained at 3-degree intervals for 15 seconds per view using a circular orbit. The energy setting was 140 Kev with a 15% to 20% window. Transaxial images were reconstructed using a Metz filter. Attenuation correction was applied using Chang's method. The reconstructed system resolution was approximately 7 mm

FWHM and was composed of cubic voxels with dimensions of 3.6 or 4.4 mm (depending on the image size). The reconstruction process created a standard series of contiguous images oriented in the transaxial, coronal, sagittal, and transtemporal planes. All patients received volumetric MR scans for coregistration with the SPECT scans. For three of patients, second time MR after second time surgery was analysed.

5.2.3 Image processing

These reconstructed transverse SPECT and MR images were transferred by disk to our laboratory where the registration, normalisation, and calculation of difference images was carried out on a SUN Sparc workstation. The final images were constructed on this workstation with commercial image analysis software packages (Analyze/AVW, Biomedical Imaging Resource, Mayo Foundation, Rochester, MN) and Woods' software using a semi-automated technique.

Previous validation of this method in partial epilepsy patients showed a median matching closer than 2.3mm using Woods' method [31]. For patients 2 and 6, the brain growth was seen as around 10% in the ictal and interictal SPECT images obtained over several months. Woods' nonlinear transformation was used. For normalisation, image calculation and analysis, and threshold change we used Analyze/AVW software. The processing was carried out using the method described in chapter 3. The normalisation was based on the mean intensity for each slice excepted the lesion and the 2SD above zero was used to threshold the foci of the lesions. The subtraction images were registered with the MR images using the Woods' and visual methods. The registered subtracted SPECT images were fused with MR images using Analyze/AVW software.

5.2.4 Comparison with visual, EEG, MR location and surgical outcome

The result is compared with the traditional visual side-by side comparison of ictal and interictal scans. The results of the traditional method of evaluating SPECT scans were compared with those of subtraction image with regard to the proportion of patients in whom images were lesion localising. The comparison were correlated with the surgical outcome.

Eight patients had ictal scalp-EEG and five patients had intracranial EEG. MR and ictal/interictal SPECT were obtained by review of their reports for all cases. Localisation by final result was compared with localisation by traditional evaluation of SPECT images and according to their percent agreement with scalp EEG localisation, intracranial EEG localisation, and with MR localisation.

Outcome of epilepsy surgery in patients who had at least 12 months of postsurgical

follow-up was assessed. Patients with seizure free or non disabling nocturnal seizure were considered as having excellent outcome, and those with an improvement of condition (greater than 75% reduction in seizure frequency) were considered to have had a good response. Otherwise was the outcome considered bad. The surgical decision, including the selection of the site of surgery, were based on information from the clinical history, MR, EEG in selected cases. The final result images were all constructed after surgery.

For patients whose final subtraction image localisation was compared with the result of surgery, the comparison was made with regard to the following outcome: Postoperative seizure free where the result was excellent; a change in the seizure rate where the result was good; and the continued presence of postoperative seizures where the result was bad after the first and second operations.

5.3 Results

Fig 5.1, 5.2, 5.3 show the results of our registration and image processing technique for three patients. In the pictures, the entire set of images were registered to each other. The image labeled ictal, shows a selected slice of the patient's SPECT perfusion scan acquired after injecting HMPAO during seizure. The image labeled interictal shows the corresponding SPECT slice acquired in the same patient at a later time after no seizures had occurred for 24 hours. The image labeled "subtracted" is a slice, corresponding to the image which is ictal minus interictal image. MR images are shown in these pictures. The subtraction image threshold greater than 2SDs above zero were fused to MR image to demonstrate how the lesions correspond to the anatomy image. Table 5 give more details about EEG, MR and SPECT ictal/interictal locations, comparison with the final subtraction images and surgical outcome.

5.3.1 Comparison of image subtraction with ictal visual assessment and correlation with surgery outcome

Eleven patients underwent epilepsy surgery, three of them had secondary surgery and had at least 12 months postsurgical follow-up. The site of surgery was temporal in 9 (81.1%) and extratemporal in 2 (19.2%). All the patients had structural abnormality detected preoperatively by MR. Four patients after one operation and one patient after secondary surgery had an excellent results (45.5%). Five patients after one operation and one patient after secondary surgery had an good results (45.5%). One patient had two times surgeries and had bad results (9.1%).

Table 5 shows an analysis of the postsurgical outcome of patients in whom the ictal and subtraction image lesions localisation were concordant with the site of surgery and those in

whom they were nonconcordant or nonlocalising. Concordance between subtraction image localisation and the site of surgery was associated with a greater likelihood of both an excellent and a good outcome. When we compare ictal SPECT image assessment with the image subtraction technique for cases for which the surgery failed, the image subtraction gave better seizure location in six patients. Moreover the technique showed a lesion reduction postsurgery, which on following secondary surgery stopped the seizures.

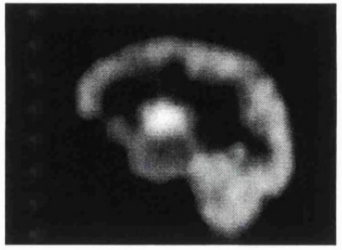

A(ictal)

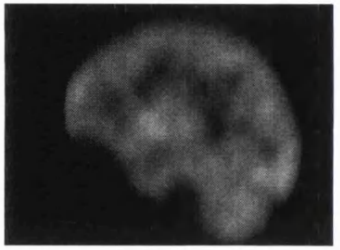

B(interictal)

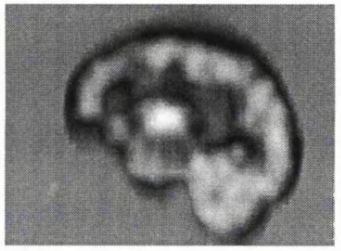

C(subtracted image from A to B)

D(greater than 2SD above 0)

E(MR before surgery)

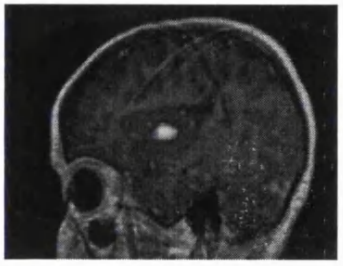

F(D fused with E)

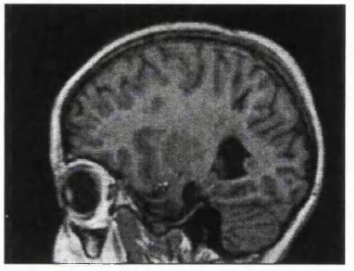

G(MR after surgery)

Fig5.1 (patient 2)

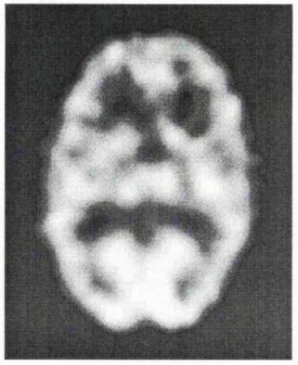

A (ictal)

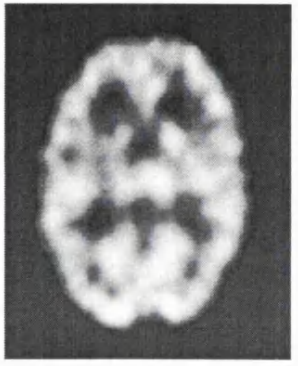

B (interictal)

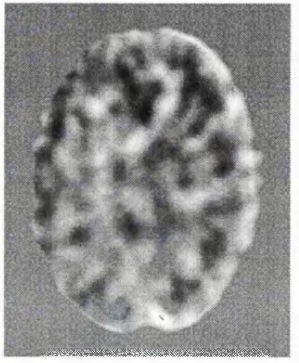

C (subtracted image from A to B)

D (greater than 2SD above 0)

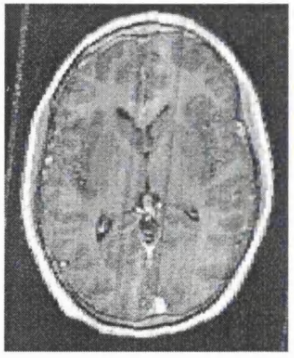

E (MR before surgery)

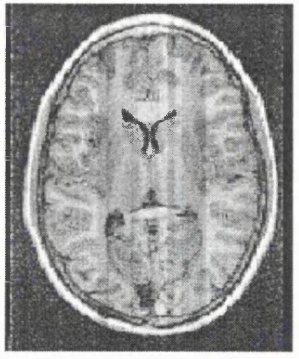

F (MR after surgery)

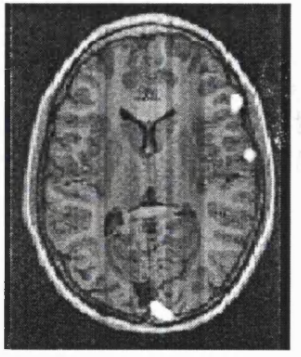

G (D fused with G)

Fig 5.2 (patient 4)

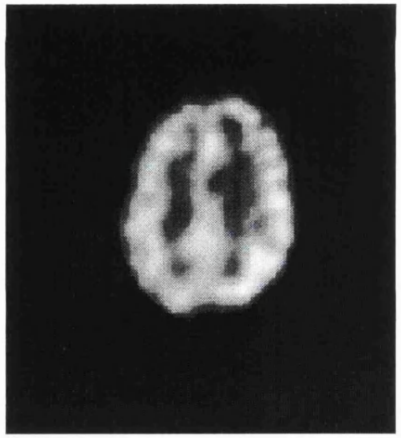

A (ictal)

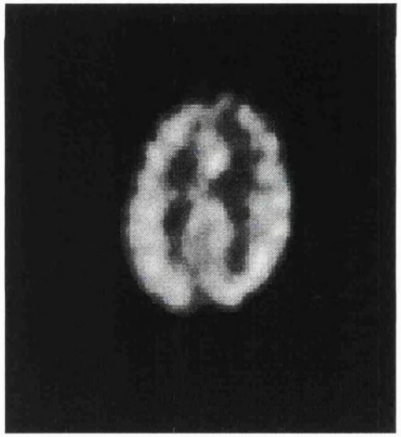

B (interictal)

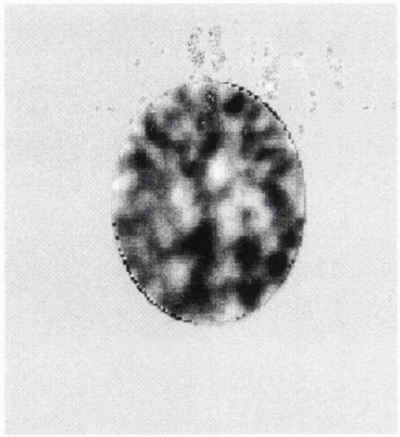

C (subtracted image from A to B)

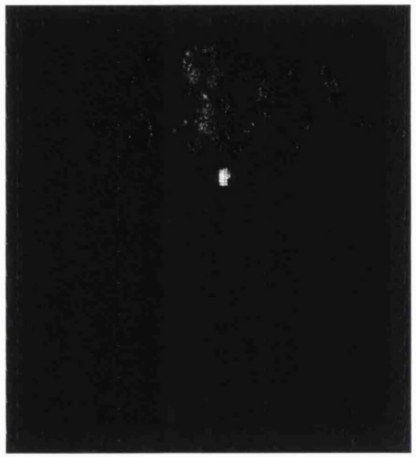

D(grater than 2SD above 0)

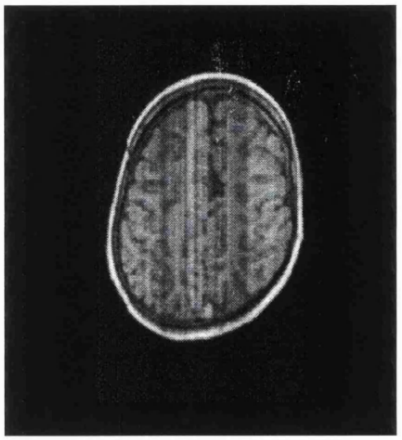

E(MR after surgery)

Fig 5.3 (patient 5)

Table 5

Seizure Site localisation Data

Patient	Depth or scalp EEG	MR Location	MR Diagnosis	Surgery Location	Surgery Outcome	Ictal	Inter-ictal	Final result image
1	LPT(d)	RPT	Dysplasia	RPF+RPT	E	RPF+RPT	RPT	RPF+RPT
2	RPT (s)	RPT	Hippocampus Atrophy	RPT(f) LPT(s)	G(f)E(s)	RPT	RPT	RPT + LPT
3	RPT(d,s)	RPT	Hippocampus Atrophy	RPT(f) LPT(s)	G(f)G(s)	PT+LPT	RPT	RPT+LPT+RF
4	LPO(s)	LPO	Dysplasia	PO(f) LPPa(s)	B(f)B(s)	RF	N	RPO+RF
5	RFPa (d)	RFPa	Tubero-sclerosis	RFPa	E	RFPa	RFPa	RFPa
6	RT(s)	LT	Tubcia-sclerosis	LT	G	LT+RC	LT+LPF	LT+LPF+RC
7	LPT(d)	LPT	glioma	LPT	E	LPT	LPT	LPT
8	LPT(s)	RPT	Hippocampus Atrophy	LPT	G	LPT+LPPa	LPT	LPT +LPPa
9	LPO(s)	LPT	Tubero-sclerosis	LPT	G	LPT	LPT+LO	LPT+LF+RC
10	RPT(s,d)	RPT	Hippocampus Atrophy	RPT	E	RPT	RPT	RPT
11	LPT(s)	LPT	Hippocampus Atrophy	LPT	G	LPT	LPT	LPT +LPa

R = right; L = left; T = temporal; Pa = parietal; O = occipital; F = frontal; E = excellent; B = still seizure; G = seizure reduced; P = posterior; C = cerebellum s = EEG surface method d = EEG depth method.

5.3.2 Comparison with MR and EEG

For MR, it is report that the location of space-occupying lesions is highly correlated with seizure onset, as judged by very high rates of seizure cessation when the structural lesion is resected . As mentioned before, hippocampal atrophy can be identified on the side of the seizure focus in up to 75% of patients with TLE. Reduced hippocampal volume on MR has been shown to predict good seizure control and a low risk of developing short-term memory difficulties after operation. In our test, five patients have diagnostic hippocampal atrophy and for two patients (10,11) the subtraction image corresponded to the MR locations and for patients 2 and 3, the MR result only corresponds partially with the subtraction image and the surgery outcome showed the seizure reduced. For patient 8, the MR location doesn't correspond to the lesion location based on surgery outcome. For five patients (patient 1,4, 5, 6 and 9), the MR diagnoses are dysplasia and tuberosclerosis. Four of these MR images showed the lesions which are included in the subtraction image. But this was not the case for patient 4. MR correctly located three patients seizure causing lesions, partly located the in six patients' cases and didn't locate them in two patients.

During surgery, lesion location was mostly based on guiding neuroimaging and scalp and depth EEG. It is reported that ictal scalp EEG and depth EEG studies agreed on the hemisphere of seizure onset in 48% and lobe of seizure onset in 29% of the cases. When grouped by lobe of seizure onset, ictal scalp EEG and depth EEG studies agreed on lateralization in 58% of studies from patients with temporal seizure onset and in 18% of studies from patients with frontal seizure onset (n= 24) [36]. In our study, 63.5% scalp or depth EEG results correspond with the surgery results which have excellent or good results.

5.4 Discussion

I reasoned that a method to demonstrate the functional change from the interictal to ictal state would result in increased sensitivity of diagnosis. This is especially significant for paediatric neurologists, because the age-dependent perfusion changes that result from brain maturation make paediatric images more difficult to read than those of adults.

The change in perfusion observed between ictal and interictal scans of patients were obtained by using image arithmetic techniques. The transformed, normalised interictal images were subtracted from the normalised ictal images to create an image where the value for each pixel represents the intensity difference between the two data sets. The significance of multiple foci of hyperperfusion present in some patients is in question. Depending more or less on the threshold selected. The standard deviation (SD) of the distribution of the subtraction pixel intensities was calculated, and the subtraction image thresholded to display only pixels with values greater than 2SDs above zero. Using this method has correctly located lesions in most cases (10 of 11).

SPECT perfusion scans are traditionally analyzed by visually comparing each cerebral region with

the homologous region of the contralateral hemisphere. This method has the immediate drawback that diffuse, symmetric, monotonic, bilateral changes in perfusion cannot be appreciated. Hence, perfusion scans performed in some patients with partial seizures do not demonstrate localising or lateralizing features when analyzed in this manner. The potential difficulties that arise when ictal, and interictal perfusion scans are compared in the conventional manner include: a.) the lack of normalization of the two studies, arising from differing quantities of injected radiopharmaceutical in the two studies or differences in the amount of time that has elapsed between injection of the radiopharmaceutical and acquisition of the scan; b.) the inability to accurately compare images slice by slice, arising from differences in patient positioning during the two studies; c.) the lack of a quantitative assessment of the difference between the two sets of images; and d.) the limited ability of perfusion scans to demonstrate anatomy. Interictal SPECT often shows hypoperfusion and an ictal study is expected to reflect increased blood flow to the area of seizure onset. These changes might be inaccessible to visual scrutiny because of their degree or distribution, or because comparison of unnormalized scans is not appropriate. Our results demonstrate that a final subtraction image localises seizures in a substantially higher proportion of patients than does the traditional method of evaluating SPECT scans. The superiority of final image subtraction method is also supported by the finding that there was no instance in which final result image was not localising, and yet for the traditional method this was not the case.

Another important point is our demonstration that, in this group of patients, the final subtraction image localised more frequently than either scalp ictal EEG or seizure-protocol MR. Nonetheless, we have demonstrated that in these patients subtraction images frequently localised the seizures when scalp ictal EEG and MR failed to do so. Nonetheless, more evidence is needed to determine whether this method can be used in selected clinical situations to reduce the need for intracranial electrode implantation. At the current time, a more appropriate application of the technique is in guiding the location and the extent of intracranial electrode implantation. Intracranial electrodes record only from a limited portion of the brain. The foci found by image subtraction can serve as a target for stereotactic implantation of intracranial electrodes to record and confirm seizure onset. The use of this method has the potential of improving the yield of intracranial EEG recording and of reducing the extent of its invasiveness.

Our results indicate that this method has greater specificity in identifying the surgically important epileptogenic zones than the traditional method of evaluating SPECT, EEG and MR. Concordance between final subtraction image localisation and the site of surgery predicted improvement in postsurgical seizure outcome, whereas the traditional SPECT , MR and EEG method did not. Therefore, although our findings cannot necessarily be extrapolated to all patients with intractable partial epilepsy, they do provide strong evidence that subtraction images give useful additional information in the presurgical evaluation of patients with complex epilepsy.

5.5 Conclusion

The aim of this project was to find the advanced way to locate the lesion in epilepsy patients using ictal and interictal SPECT images. My study indicates that the subtraction image method improves the sensitivity and the specificity of SPECT in localising the seizure focus in intractable epilepsy patients. This method can provide localising information when EEG and MR cannot. Furthermore, concordance between subtraction image localisation and the site of surgery independently predicts improvement in the occurrence of seizures after epilepsy surgery. This study, which focuses on children, shows this method can be applied successfully to such a population.

Chapter 6.
Ideas for future research

6.1 The further methodology study

If we look at the method carefully, we can see there are some processes that need further to be modified during the calculation process. Nor it is clear that normalisation based on total counts in the brain slices is the best method for pre-processing the SPECT data before calculating difference images. The normalisation is complicated by the fact that extraction fraction of HMPAO becomes non-linear at flow rates above 55 ml/min/100g [36]. There is no report comparing different normalisation methods. We propose to investigate other normalisation schemes and compare these with the one we used. In another proposed normalisation scheme, we will normalise the SPECT data according to concentration levels found in the cerebellum. Yet another scheme suggests that the brain stem may be the structure to which radio-pharmaceutical uptake can be best normalised. The statistical analysis based on histogram distribution of the subtracted and normalised ictal and interictal images help to clarify the results.

6.2 Using this method for post-ictal study

The regional hyperperfusion observed on ictal SPECT is generally believed to be a consequence rather than a cause of seizure activity. Thus, one would expect CBF changes to occur simultaneously or after the onset of ictal electrographic activity. However, recent studies using invasive long-term cortical CBF monitoring have demonstrated that rCBF changes occur up to 20 min prior to ictal EEG onset on subdural strip electrodes. Initially at 10~ 20 min before seizure onset, there is already a gradual increase in rCBF in the epileptic temporal lobe. At the time of seizure onset, there is an abrupt and brief drop in CBF, followed quickly by an increase of rCBF in the whole temporal lobe during the seizure.

The timing of radioisotope injection is critical to the sensitivity and the specificity of the SPECT. Two other studies found that ictal injection times were later in patients with non localising or falsely localising results than they were in patients with localising results[37] [68]. When the injection is early, there is a greater likelihood that the predominant seizure activity will be centred focally around the epileptogenic zone, and a correctly localised SPECT image will result. However, when the ictal injection is late there is more time for secondary areas to be affected by perfusion changes. This may result in a poorly or a falsely localised scan.

Post-ictal SPECT is defined as an injection later than 30 sec post-seizure completion with seizure monitoring. Previous studies reported that there is a post-ictal switch when blood flow in the epileptogenic zone rapidly converts from hyper-perfusion to hypo-perfusion. The time of radio-tracer

injection when conversion first occurs has been estimated to be between 0 and 60 seconds after the end of temporal lobe seizures. The timing of the switch after extratemporal seizures is even less well-studied, but anecdotal information suggests that it may be earlier than it is after temporal lobe seizures.

We need to investigate whether the time of radiotracer injection in patients with hyperperfusion-dominant in final subtraction images or hypoperfusion-dominant in these images, and which threshold selection scheme are more suitable for the late ictal injection and post-ictal for the children.

6.3 Lesion size and threshold selection

Clinically, the size of the lesion is another important issue for the surgery. The areas of apparent lesion depend on the threshold selection. What is the correct choice of threshold? This question needs further investigation.

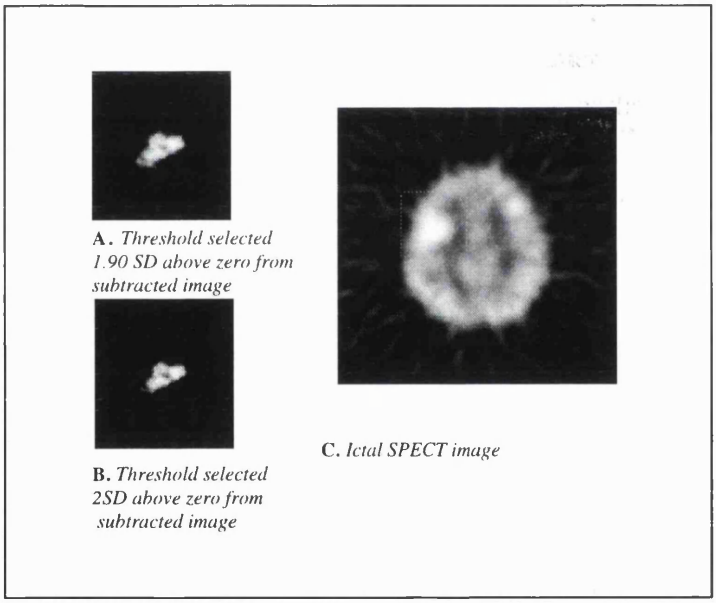

Fig 6.1 *Different threshold selected images from subtracted image.*

From Fig 6.1, we can see that apparent lesion sizes depend on the threshold. The threshold selection scheme needs to be studied by post-surgical SPECT examination. Not only for the location but also for the size. Correctly determining the size of lesions will more useful for the surgery. This question need further investigation.

References

[1] Woods RP "MRI-PET registration with automated algorithm" Journal of Computer Assisted Tomography, 17(4): 536-546, July/August 1993.

[2] Studholme C, Hill DLG, Hawkes DJ "Automated three-dimensional registration of magnetic resonance and positron emission tomography brain images by multiresolution optimization of voxel similarity measures" Med Phy, 24(1), January 1997.

[3] Correia JA "Registration of Nuclear Medicine Images" The Journal of Nuclear Medicine, Vol 31, No 7, July 1990.

[4] Van den Elsen PA, EJD Pol, Viergever MA "Medical image matching- A review with classfication" IEEE engineering in Medical and Biology, Vol 12, Match 1993.

[5] VoÜte PA, Kalifa C, Barrett A "Cancer in Children" Oxford University Press, 1998.

[6] William JR, Thwaites DI "Radiotherapy physics in practice" Oxford University Press, 1993.

[7] Faber TL, McColl RW, Opperman RM, Corbett JR, Peshock RW "Spatial and temporal registration of cardiac SPECT and MR images: methods and evaluation" Radiol, 179(3): 857-861, 1991.

[8] Richard LW " 'Autometabolic' tumor imaging: Fusion of FDG-PET with CT or MRI to localize foci of increased activity" Journal of Nuclear Medicine, Vol 34, No 7, July 1993.

[9] Shukla SS, Honeyman JC, Crosson B, Williams CM, Nadeau SE "Method for registering brain SPECT and MR Images" J Comput Assist Tomogr, Vol 16, No 6, 1992.

[10] Pietrzyk U, Herholz K, Heiss W-D "Three-dimensional alignment of functional and morphological tomograms" J Comput Assist Tomogr, 14(1): 51-59, January/February 1990.

[11] Seitz RJ, Bohm C, Greitz T, Roland PE, Eriksson L, Blomqvist G, Rosenqvist G, Nordell B "Accuracy and precision of the computerized brain atlas programme for localization and quantification in position emission tomography" J Cerebr Blood Flow Metab, 10(4):443-447, 1990.

[12] Maguire Jr GQ, Noz ME, Rusinek H, Jaeger J, Kremer EL, Joseph JS, Gwenn S "Graphics applied to medical image registration" IEEE Comp Graph Appl, 11(2):20-28, 1991.

[13] Kapouleas I, Alavi A, Alves WM, Gur RE, Weiss DW "Registration of 3-dimensional MR and PET images of the human brain without markers" Radiol, 181(30):731-739,1991.

[14] Yaorong Ge "Retrospective registration of PET and MR brain images: An algorithm and its stereotactic validation" J Comput Assist Tomogr, Vol 18, No 5, 1994.

[15] Evans AC, Dai W, Collin L, Neelin P, Marrett S "Warping of a computerized 3-D atlas to match brain image volumes for quantitative neuroanatomical and functional analysis" SPIE, Vol 1445 Image Processing, 1991.

[16] Hill DLG, Hawkes DJ, Crossman JE, Gleeson MJ, Cox TCS, FRCR, Bracey EECM, Strong AJ, FRCS, Graves P, DCR "Registration of MR and CT images for skull base surgery using point-like anatomical feature" Brit J Radio, 64(767): 1030-1035, 1991.

[17] Uwe P, Herholz A, Schuster H, Stockhausen V, Lucht H, Heiss W "Clinical applications of registration and fusion of multimodality brain images from PET, SPET, CT, and MRI" Euro Jour of Radio, 21 174-182, 1996.

[18] Sarah JN, Mark RD Paul JB, Lawrence LW, Thomas FB, Randall H, William PD, Stephen H, Michael DP, Susan C, Daniel BV "Alignment of tumor MR images and high resolution [18F]Fluorodeoxyglucose PET images for the evaluation of patients with brain tumors" J Comput Assist Tomogr, 21(2):183-191, 1997.

[19] Pelizzari CA, Chen GTY, Spelbring DR, Weichselbaum RR, Chin-Tu C "Accurate three-dimensional registration of CT, PET, and /or MR images of the brain" J Comput Assist Tomogr, Vol 13, No 1, 1989.

[20] Alpert NM, Bradshaw JF, Kennedy D, Correia JA "The principal axes transformation- a method for image registration" J Nucl Med, Vol 31:1717-1722, 1990.

[21] Meltzer CC, Jeffrey PL, Helen SM, Henry NW, Jr, J JF "Correction of PET data for partial volume effects in human cerebral cortex by MR imaging" J Comput Assist Tomogr, Vol 14(4):561-570, 1990.

[22] Satoshi M, Kevin LB, Kien SL, Mark AM "An automated method for rotational correction and centering of three-dimensional functional brain images" J Nucl Med, Vol 33:1579-1585, 1992.

[23] William G, Bradley Tr, Graema M Bydder "Advanced MR imaging technique" Martin Dunitz Ltd, 1997.

[24] Hill DLG, Hawkes DJ, Gleeson MJ "Accurate frameless registration of CT image of the head: Applications in planning surgery and radiation therapy" Radiology, 191, 447-454,1994.

[25] John WH "Three-dimensional hippocampal MR morphometry with high-dimensional

transformation of a neuroanatomic atlas" Radiology, 202:504-510, 1997

[26] Lothar RS, Rober B, Wolfgang S Gunter HH, Volker S, Ludwig GS, Walter JL "Three dimensional image correlation of CT, MR, and PET studies in radiotherapy treatment planning of brain tumors" Journal of Computer Assisted Tomography, 11(6): 948-954 November/December 1987.

[27] Elissa LK, Marilyn EN "CT-SPECT fusion for analysis of radiolabeled antibodies: Applications in gastrointestinal and lung carcinoma" Nucl Med Biol, Vol 18, No 1, pp 27-42, 1991.

[28] Loats H "CT and SPECT image registration and fusion for spatial localization of metastatic processes using radiolabled monoclonals" Journal of Nuclear Medicine, Vol 34, No 3, March 1993.

[29] Andrew MS , Homer M, Jiaju Z, Farhad D, Hatalie M, Hovanes K, Geoge S, Martin AG, Katherine K, Samuel DJY, Eseng L, Stanlry JG, Steven ML "Image registration of SPECT and CT images using an external fiduciary band and three-dimensional surface fitting in metastatic thyroid cancer" Journal of Nuclear Medicine, Vol 36, No 1, January 1995.

[30] Hill DLG, Hawkes DJ, Hussain Z, Green SME, Ruff CF, Robinson GP "Accurate combination of CT and MR data of the head: A validation and applications in surgical and therapy planning" Computerized Medical Imaging and Graphics, Vol 17(4/5), pp. 357-363, 1993.

[31] http: // www.vuse.vanderbilt.edu/~image/registration.

[32] Koop M "Volumetric Development of the Fetal Telencephalon, Cerebral Cortex, Diencephalon, and Rhombencephalon Including the Cerebellum in Man" Bibthca anat., No 28, pp. 53-78(Karger, Basel 1986).

[33] http://www.mayo.edu/bir/AVW/Introduction.html.

[34] O'Donohoe NV "Epilepsies of childhood" Butterworth-Heinemann Oxford , 1994.

[35] Murray IPC, Ell PJ "Nuclear medicine in clinical diagnosis and treatment" Churchill Living Stone ,1998.

[36] Zubal GI, Susan SS, Khursheed I, John S, Eileen OS, Gary W, Paul BH "Difference images calculated from ictal and interictal Technetium-99m-HMPAO SPECT scans of epilepsy" The Journal of Nuclear Medicine, Vol 36, No 4, April 1995.

[37] T.J. O'Brien, MB BS, FRACP; E.L. So, MD; B.P.Mullan, MB CHB, FRACP; M.F. Hauser, MD; B.H. Brinkmann, BS; N.I. Bohnen, MD, PhD; D, Hanson, BS; G.D. Cascino, MD; C.R. Jack,

Jr., MD; and F.W. Sharbough, MD "Subtraction ictal SPECT co-registered to MRI improves clinical usefulness of SPECT in localizing the surgical seizure focus" Neurology 1998

[38] Van H M, Kooy H.M "Automatic three-dimensional correlation of CT-CT, CT-MRI, and CT-SPECT using chamfer matching" Medical Physics, 21:1163-1178, 1994.

[39] Hill DLG, Hawkes DJ, Harrison NA, Ruff CF "A strategy for automated multimodality image registration incorporating anatomical knowledge and imager characteristics" In Proceeding of information processing in medical imaging ,182-196, 1993.

[40] David NL, Xiaoping Hu, Kim KT, Simranjit C, Charles AP, George TYC, Robert NB, Chin-Tu C, Dlalcolm DC, John FM, Javad H, Jean PS "The brain: intergrated three-dimensional display of MR and PET images" Radiology 1989; 172:783-789

[41] Jeffrey NY, Frederic HF, Howard DG, Cathy GE, Beth AH, Charles AP, John WK "Intermodality, retrospective image registration in the thorax" J Nucl Med 1995; 36:2333-2338.

[42] Rik Stokking "Integrated visualization of functional and anatomical brain images" KEMA, Shell international exploration and production, and ADAC Europe

[43] Stefan E, Iwao K, Roger RF, Anneke R, Brain FH, Michael JF "Automated study image registration technique for SPECT and PET" J Nucl Med 1996: 37:137-145

[44] Imran MB, Kawashima R, Awata S, Sato K, Kinomura S, Ono S. Yoshioka S, Sato M Fukuda H " Parametric mapping of cerebral blood flow deficits in Alzheimer's disease: a SPECT study using HMPAO and image standardization technique" J Nucl Med 1999 Feb: 40(2): 244-9

[45] Imran MB, Kawashima R, Awata S, Sato K, Kinomura S, Ito H, Koyama M, Goto R, Ono S, Yoshioka S, Fukuda H "Mean regional cerebral blood flow images of normal subjects using technetium-99m-HMPAO by automated image registration" J Nucl Med 1998 Jan: 39(1): 203-7

[46] Hill DLG, Studholme C, Hawkes DJ "Voxel similarity measures for automated image registration" In proceeding of visualisation in biomedical computing" Vol SPIE 2359, 205-216, 1994

[47] Collignon A, Vandermeulen D, Suetens P, marchal G, Baert A, Oosterlinck A "Automatic registration of 3D images of the brain based on fuzzy objects" In proceeding of medical imaging" 195-204 ,1995

[48] Meyer CR, Boes JL, Kim B, Bland PH, Zasadny KR, Kison PV, Koral K, Frey KA, Wahl RL "Demonstration of accuracy and clinical versatility of mutual information for automatic multimodality image fusion using affine and thin-plate spline warped geometric deformation" Med

Imag Anal ; Apr; 1(3): 195-206 1997

[49] Kim B, Boes JL, Bland PH, Chenevert TL, Meyer CR " Motion correction in fMRI via registration of individual slices into an anatomical volume" Magn reson Med 41(5): 964-72 May 1999

[50] Golfinos JG, Fitzpatrick BC, Smith LR, Spetzler RF " Clinical use of a frameless stereotaxic arm- results of 325 cases" Journal of neurosurgery ; Vol 83, No 2, 197-205, 1995

[51] Grimson WEL, Ettinger GJ, White SJ, Lozanoperez T, Wells WM, Kikinis R "An automatic registration method for frameless stereotaxy, image guided surgery, and enhanced reality visualisation" IEEE Transactions on medical imaging Vol 15, No 2, 129-140

[52] Cai J, Chu JC, Recine D, sharma M, Nguyen C, Rodebaugh R, Saxena VA, Ali A "CT and PET lung image registration and fusion in radiotherapy treatment planning using the chamfer - matching" Int-J-Radiat-Oncol-Biol-Phys 43(4): 883-91, Mar 1 1999

[53] Munley MT, Marks LB, Scafone C, Sibley GS, Patz EFJ, Turkington TG, Jaszczak RJ, Gilland DR, Anscher MS, Gilland DR "Multimodality nuclear medicine imaging in three-dimensional radiation treatment planning for lung cancer: challenges and prospects" Lung-Cancer 23(2):105-14 Feb, 1999

[54] Rosenman JG, Miller EP, Tracton G, Gullip TJ "Image registration: an essential part of rediation therapy treatment planning" Int-J-Radiat-Oncol-Biol-Phys 40(1): 197-205, Jan 1998

[55] Ernst T, Chang L , Ltti L, Spect O "Correlation of regional cerebral blood flow from perfusion MRI and spect in normal subjects" Magn-Reson-imaging 17(3): 349-54 Apr 1999

[56] Imran MB, Kawashima R, Awata S, Sato K, Kinomura S, Ono S, Sato M, Fukuda H " Tc-99m HMPAO SPECT in the evaluation of Alzheimer's disease: correlation between neuropsychiatric evaluation and CBF images" J Neurol Neurosurg Phychiatry 66(2): 228-32 , Feb 1999

[57}Kozinska D, Tarnecki r, Nowinski K "Presention of brain electrical activity distribution on its cortex surface derived from MR images" Technol Health Care (2-3): 209-24, Sep 1998

[58] Brinkmann BH, O'Brien TJ, Aharon S O'Connor MK, Mullan BP, Hanson DP, Robb RA " Quantitative and clinical analysis of SPECT image registration for epilepsy studies" J Nucl Med 40(7): 1098-105 Jul 1999

[59] Woods RP, Grafton ST, Watson JD, Sicotte NL, Mazziotta JC "Automated image registration: II Intersubject validation of linear and nonlinear models" J Comput Assist Tomogr 22(1):

153-65, Jan-Feb 1998

[60] O'Brien TJ, O'Connor MK, Mullan BP, Brinkmann BH, Hanson D, Jack CR,So EL "Subtraction ictal SPECT co-registered to MR in partial epilepsy: description and technical validation of the method with phantom and patient studies" Nucl Med Commun 19(1): 31-45 Jan 1998

[61] Pierre V, Anna K, Cecile C, Andreas H, Jean LS, Isabelle G, Dorothe V, Jean FM, Perrine P, Olivier D, Catherine C "Use of subtraction ictal SPECT co-registered to MRI for optimizing the localisation of seizure foci in children" J Nucl Med 40:786-92 1999

[62]Collignon A, Vandermeulen, Suetens p, and Marchal G "3D multi-modality medical image registration using feature space clustering" In Proceedings of the 1st international conference on computer vision, virtual reality and robotics in medicine. 195-204. Spinger-Verlag, 1995.Nice

[63]Studholme C, Hill D L G, and Hawkes D J "Multiresolution voxel similarity measures for MR-PET registration" Proceedings of information processing in medical imaging, 287-298, 1995, France

[64]Zinreich SJ, Watcuabe T, Manaka S, et al "Frameless stereotaxic integration of CT imaging data: accuracy and initial applications" Radiology 188: 735-742, 1993

[65] Kortmann, RD "Precision and acute toxicity of craniospinal irradiation in malignant brain tumours in childhood: Preliminary results of the quality assurance program of the German prospective cooperative study HIT' 91" Children's hospital of the university of Wurzburg, Germany

[66] Roland W, Michael S "Image segmentation and uncertainty" Research studies press LTD, 1998

[67] Fitzpatrick JM, Hill DLG, Shyr Y, West J, Studholme C, and Maurer CR " Visual assessment of the accuracy of retrospective registration of MR and CAT images of the brain". IEET Transactions on medical image, Vol 17, No 4, August 1998

[68] O' Brien TJ, Mullan BP, Hauser MF, Brinknann BH, Jack CR, Cascino GD, Meyer FB, and Sharbrough FW "Subtraction SPECT co-registered to MRI improves postictal SPECT localization of seizure foci" Neurology 1999; 52:137-146

[69] Woods RP, Mazziotta JC, and Cherry SR "A rapid automated algorithm for accurately aligning and reslicing PET images" Journal of Computer Assisted Tomography 16: 620-633, 1992.